

1 Archaeal Intact Polar Lipids in Polar Waters: A Comparison Between 2 the Amundsen and Scotia Seas

3 Charlotte L. Spencer-Jones¹, Erin L. McClymont¹, Nicole J. Bale², Ellen C. Hopmans²,
4 Stefan Schouten^{2,3}, Juliane Müller⁴, E. Povl Abrahamsen⁵, Claire Allen⁵, Torsten
5 Bickert⁴, Claus-Dieter Hillenbrand⁵, Elaine Mawbey⁵, Victoria Peck⁵, Aleksandra
6 Svalova⁶, James A. Smith⁵

7 ¹Department of Geography, Durham University, Lower Mountjoy, South Road, Durham, DH1 3LE, UK.

8 ²NIOZ Royal Netherlands Institute for Sea Research, Department of Marine Microbiology and
9 Biogeochemistry, P.O. Box 59, 1790 AB Den Burg, Texel, The Netherlands.

10 ³ Department of Earth Sciences, Utrecht University, Utrecht, The Netherlands.

11 ⁴Alfred Wegener Institute, Helmholtz Center for Polar and Marine Research, 27568 Bremerhaven, Germany.

12 ⁵British Antarctic Survey, High Cross, Madingley Road, Cambridge, CB3 0ET, UK.

13 ⁶ School of Natural and Environmental Sciences, Newcastle University, Newcastle-upon-Tyne, NE1 7RU,
14 UK.

15 Correspondence to: Charlotte L. Spencer-Jones (charlotte.spencer-jones@open.ac.uk)

16 Abstract

17 The West Antarctic Ice Sheet (WAIS) is one of the largest potential sources of future sea-level rise, with
18 glaciers draining the WAIS thinning at an accelerating rate over the past 40 years. Due to **difficulties**
19 **complexities** in calibrating palaeoceanographic proxies for the Southern Ocean, it remains difficult to assess
20 whether similar changes have occurred earlier during the Holocene or whether there is underlying centennial
21 to millennial scale forcing in oceanic variability. Archaeal lipid – based proxies, specifically Glycerol
22 Dialkyl Glycerol Tetraether (GDGT; (e.g. TEX₈₆ and TEX₈₆¹) are powerful tools for reconstructing ocean
23 temperature, but these proxies have been shown previously to be difficult to apply to the Southern Ocean. A
24 greater understanding of the parameters that control Southern Ocean GDGT distributions would improve the
25 application of these biomarker proxies and thus help provide a longer-term perspective on ocean forcing of
26 Antarctic ice sheet changes. In this study, we characterised intact polar lipid (IPL) - GDGTs, representing
27 (recently) living archaeal populations in suspended particulate matter (**SPM**) from the Amundsen Sea and the
28 Scotia Sea. **SPM samples from the Amundsen Sea were collected from up to 4 water column depths**
29 **representing the surface waters through to Circumpolar Deep Water (CDW) whereas the Scotia Sea samples**
30 **were collected along a transect encompassing the sub-Antarctic front through to the southern boundary of the**
31 **Antarctic Circumpolar Current. IPL-GDGTs with low cyclic diversity were detected throughout the water**
32 **column with high relative abundances of hydroxylated IPL-GDGTs identified in both the Amundsen and**

33 Scotia Seas. Results from the Scotia Sea show shifts in IPL-GDGT signatures across well-defined fronts of
34 the Southern Ocean. Indicating that the physicochemical parameters of these water masses determine
35 changes in IPL-GDGT distributions. The Amundsen Sea results identified GDGTs with hexose-
36 phosphohexose head groups in the CDW suggesting active GDGT synthesis at these depths. These results
37 suggest that GDGTs synthesized at CDW depths may be a significant source of GDGTs exported to the
38 sedimentary record and that temperature reconstructions based on TEX₈₆ or TEX₈₆^L proxies may be
39 significantly influenced by the warmer waters of the CDW. Shifts in IPL-GDGT signatures across well-
40 defined fronts of the Southern Ocean revealed a correlation between the physicochemical parameters of these
41 water masses and IPL-GDGT distributions. Further analysis is required to elucidate the additional role of
42 productivity and nutrient availability on Southern Ocean IPL-GDGT distributions. Of particular note for
43 proxy development in the Amundsen Sea is that IPL-GDGTs are likely actively synthesised at Circumpolar
44 Deep Water depths and may be a significant source of GDGTs exported to the sedimentary record in this
45 region.

46 Key words

47 Southern Ocean, Intact Polar Lipid (IPL), Glycerol Dialkyl Glycerol Tetraether (GDGT), Amundsen Sea,
48 Scotia Sea, Circumpolar Deep Water, Archaea, Thaumarchaeota.

49 **1. Introduction**

50 Over the past ca. 50 years the West Antarctic Ice Sheet (WAIS) has lost ice mass at an accelerating rate with
51 some suggesting that the complete collapse of the WAIS may already be underway (Joughin et al., 2014;
52 Mouginit et al., 2014; Rignot et al., 2019). The WAIS is grounded below sea level and the edges of the ice
53 sheet are floating ice shelves that are, highly sensitive to changes in ocean properties. Widespread ice
54 sheet/shelf thinning will likely have influence on biogeochemical cycling through ocean productivity
55 (Raiswell et al., 2008; Menviel et al., 2010; Wadham et al., 2013), carbon reservoirs and carbon
56 sequestration (Yager et al., 2012; Wadham et al., 2019), in addition to sea ice and ocean circulation changes
57 (Menivel et al., 2010).

58 One of the challenges in understanding and predicting the behaviour of WAIS is a lack of long-term ocean
59 temperature records (i.e. prior to the satellite era ~1992). Such records are needed to better understand the
60 links between WAIS stability, physical properties of the Southern Ocean, and biogeochemistry which might

61 vary on centennial to millennial timescales (Smith et al., 2017; Hillenbrand et al., 2017). Organic
62 geochemical proxies based on the ratios of archaeal membrane lipids can be used to reconstruct past ocean
63 temperature and biogeochemistry. Glycerol dialkyl glycerol tetraether (GDGT) lipids are particularly
64 promising with the TEX_{86} , TEX_{86}^L and OH-GDGT proxies having been widely used to reconstruct ocean
65 temperatures in tropical, temperate, and northern polar regions (e.g. Jenkyns et al., 2004; Huguet et al., 2006,
66 2011; Sinninghe Damsté et al., 2010; Darfeuil et al., 2016). In contrast, only a handful of studies have
67 successfully applied these proxies in the Southern Ocean (Kim et al., 2012; Shevenell et al., 2011; Etourneau
68 et al., 2013, 2019). This reflects a combination of low concentrations of GDGTs ~~as well as with~~ an
69 incomplete understanding of archaeal populations and habitat/niche preference (Kim et al., 2010). A better
70 understanding of the source of GDGTs in the Southern Ocean and factors that impact archaeal populations
71 could improve application of TEX_{86} based proxies in this environment.

72 **1.1. Tracing Archaea with Intact Polar Lipids**

73 Archaea are a key component of picoplankton within the polar oceans (DeLong et al., 1994; Murray et al.,
74 1998; Church et al., 2003; Kirchman et al., 2007; Alonso-Saez et al., 2008) and have an important role in
75 biogeochemical cycling and in marine food webs. GDGTs are important cell membrane components present
76 in many marine archaea (Schouten et al., 2013 and references therein) including the ammonia oxidising
77 archaea (AOA) Thaumarchaeota (previously assigned to the phylum Crenarchaeota; Brochier-Armanet et al.,
78 2008; Spang et al., 2010). Marine archaea produce isoprenoid GDGTs with a polar head group (intact polar
79 lipids - IPLs). Upon cell death the polar head group is relatively rapidly cleaved off resulting in the
80 preservation of the core GDGT lipid (c-GDGTs). c-GDGTs are subsequently preserved in the sedimentary
81 record and can be used to reconstruct Antarctic palaeoenvironmental change over long time scales (Kim et
82 al., 2012; Shevenell et al., 2011; Etourneau et al., 2013, 2019). Thaumarchaeota are a major source of
83 GDGTs to the environment with pure culture studies detecting GDGTs with 0-3 cyclopentane moieties,
84 crenarchaeol (cren, which contains 4 cyclopentane moieties and a cyclohexane moiety) and cren regio isomer
85 (cren', Schouten et al., 2000; Sinninghe Damsté et al., 2018). Other archaeal phyla (e.g. marine
86 Euryarchaeota group II) have been hypothesised as sources of GDGTs to the marine realm (Lincoln et al.,
87 2014a,b), however this source is unlikely to be significant in marine samples (Schouten et al., 2014; Zeng et
88 al., 2019; Besseling et al., 2020). Furthermore, archaea exist throughout the marine water column with

89 several studies suggesting a GDGT contribution to sediments from “deep water” Thaumarcheota (e.g. Ingalls
90 et al., 2006; Shah et al., 2008; Kim et al., 2016).

91 IPL-GDGTs may be used as proxies for tracing (recently) living archaeal populations (e.g. Pitcher et al.,
92 2011; Sinninghe Damsté et al., 2012; Elling et al., 2014, 2017). AOA enrichment cultures reveal three
93 common GDGT head groups; monohexose (MH), dihexose (DH), and hexose-phosphohexose (HPH)
94 (Schouten et al., 2008; Pitcher et al., 2010, 2011), with all three IPL head groups reported in environmental
95 samples (Lipp et al., 2008; Lipp and Hinrichs, 2009; Schubotz et al., 2009; Schouten et al., 2012; Xie et al.,
96 2014; Evans et al., 2017; Sollich et al., 2017; Besseling et al., 2018). HPHs are a common IPL in all AOA
97 enrichment cultures, to date, with MH and DH intermittently present (Pitcher et al., 2011; Elling et al., 2017;
98 Bale et al., 2019). The interpretation of IPL-GDGTs as proxies for living archaeal biomass is complicated by
99 their degradation to c-GDGTs with increasing evidence that some IPLs are preserved following cell death
100 (Bauersachs et al., 2010; Huguet et al., 2010; Schouten et al., 2010; Xie et al., 2013; Lengger et al., 2014).

101 Kinetic modelling has suggested greater preservation of glycolipids compared with phospholipids (Schouten
102 et al., 2010), therefore suggesting that HPH-GDGTs may have potential as biomarkers for living,
103 metabolically active, Thaumarchaeotal populations (Schouten et al., 2012; Elling et al., 2014, 2017).

104 However, HPH-GDGT abundance is variable across the 1.1a Thaumarchaeota clade which could make the
105 interpretation of this biomarker in environmental studies complex (Elling et al., 2017). DH-GDGTs and DH-
106 OH-GDGT on the other hand are thought to be produced exclusively by 1.1a Thaumarchaeota with more
107 uniform abundance across the clade (Pitcher et al., 2011; Sinninghe Damsté et al., 2012), and could therefore
108 be potential tracers for living Thaumarchaeota (Elling et al., 2017).

109 In this study, we present the first characterisation of IPL-GDGTs in suspended particulate matter (SPM)
110 from two locations in the Southern Ocean, the Scotia Sea and the Amundsen Sea. The first aim of this study
111 is to characterise the distributions of IPL-GDGTs within the Southern Ocean in order to expand our
112 understanding of Thaumarchaeotal distributions in Polar Regions and improve our interpretation of GDGT
113 based proxies. The second aim of this study is to understand the environmental controls on IPL-GDGT
114 distributions in the Southern Ocean. In this study, we analyse the water column profiles of IPL-GDGTs with
115 18 samples from the Amundsen Sea and ~~3015~~ samples from a transect in the Scotia and Weddell Sea.

116 **1.2. Study Area**

117 The Southern Ocean drives global thermohaline circulation and is therefore a major regulator of Earth's
118 oceans and climate (Carter et al., 2009). The clockwise flowing Antarctic Circumpolar Current (ACC)
119 connects all the major ocean basins resulting in a major role in the distribution of heat, salt, and gasses
120 (Carter et al., 2009). The surface waters of the Southern Ocean show clear shifts in water properties (salinity
121 and temperature) which mark ocean fronts, and in the present study include; Sub-Antarctic front (SAF), the
122 Polar Front (PF), the Southern Front of the ACC (SACCF), and the Southern Boundary of the ACC
123 (SBACC) (Carter et al., 2009 and references therein). Antarctic surface waters (AASW; 100m thick),
124 extending from the Antarctic continental shelf to the PF, are characterised by near freezing temperatures and
125 salinity values up to 34.3 practical salinity units (PSU), although these properties can vary on a regional basis
126 (Carter et al., 2009 and references therein). The transition between AASW south of the PF and Sub-Antarctic
127 surface water (SASW) north of the SAF occurs in the Polar Frontal Zone. Due to complex mixing processes,
128 the properties of surface water in the Polar Frontal Zone are often variable, but this water is generally
129 warmer (3–8 °C) and less dense (salinity 34–34.4 PSU) than AASW (Carter et al., 2009 and references
130 therein). Lastly, SASW is comparatively warmer (6–12 °C) with salinity >34.3 PSU (Carter et al., 2009 and
131 references therein). Circumpolar Deep Water (CDW) together with CDW derived, modified deep water
132 masses, such as Warm Deep Water in the Weddell Gyre (e.g. Vernet et al., 2019) is a key Southern Ocean
133 water mass and can be detected between ~1400 m and >3500 m depth offshore from the Antarctic continent.
134 CDW can rise to meet AASW or even outcrop along the Antarctic continental margin (Carter et al., 2009 and
135 references therein). Mixing of CDW with different water masses gives rise to two types: Upper CDW
136 (UCDW) defined by an oxygen minimum, high nutrient concentrations, and a depth of 1400–2500 m; and
137 Lower CDW (LCDW) defined by a salinity maximum of 34.70–34.75 PSU (Carter et al., 2009 and
138 references therein). In contrast to UCDW, LCDW extends south of the SBACC (Orsi et al., 1995), is
139 upwelling at the continental slope, and can protrude onto the shelf where it mixes with super-cooled shelf
140 waters, renewing LCDW and forming Antarctic Bottom Water (AABW) (Carter et al., 2009 and references
141 therein).

142 The Scotia Sea is located in the eastern Atlantic sector of the Southern Ocean (20°W to 65°W) bounded by
143 the South Atlantic Ocean to the North, the Drake Passage to the West, and by the Weddell Sea to the South

144 (Figure 1). The Scotia Sea is influenced by the eastward flow of the ACC, via the Drake Passage, and by a
145 northward component of the ACC, caused by topographic steering and northward outflow of recently
146 ventilated waters from the Weddell Sea, whereby Weddell Sea Deep Water (WSDW) is incorporated into
147 the ACC (Locarnini et al., 1993; Naveira Grabato et al., 2002a,b), thus creating a region of high mixing
148 (Heywood et al., 2002) and intense water mass modification (Locarnini et al., 1993).
149 The Amundsen Sea extends from 100°W to 130°W and is bounded by the Sub-Antarctic Pacific to the North
150 (Figure 1). The Amundsen Sea water column south of the PF mainly consist of a thin upper layer of cold and
151 fresh AASW overlying relatively warm CDW. The Amundsen Sea embayment is located offshore from one
152 of the major WAIS drainage basins and observations show a clear trend in glacial retreat over recent decades
153 (e.g. Mouginito et al., 2014; Paolo et al., 2015; Rignot et al., 2019). The deep ice shelves (extending up to
154 1000-m below sea level) surrounding the Amundsen Sea embayment are exposed to unmodified CDW which
155 can be up to 4 °C above the *in situ* melting point (Jacobs et al., 1996, 2011; Rignot and Jacobs, 2002; Jenkins
156 et al., 2010; Rignot et al., 2013; Webber et al., 2017) so that CDW may drive enhanced melt rates and ice
157 sheet instability in this region (Shepherd et al., 2001; Zwally et al., 2005; Rignot et al., 2008; Pritchard et al.,
158 2009; Wingham et al., 2009).

159 2. Methodology

160 2.1. Study Area

161 The Southern Ocean drives the global thermohaline circulation and is therefore a major regulator of Earth's
162 oceans and climate (Carter et al., 2009). The eastward flowing Antarctic Circumpolar Current (ACC)
163 connects all the major ocean basins resulting in a major role in the distribution of heat, salt, and gasses
164 (Carter et al., 2009). The surface waters of the Southern Ocean show clear shifts in water properties (salinity
165 and temperature) which mark ocean fronts, and in the present study include the: Sub-Antarctic Front (SAF),
166 the Polar Front (PF), the Southern Front of the ACC (SACCF), and the Southern Boundary of the ACC
167 (SBACC) (Carter et al., 2009 and references therein). Antarctic surface waters (AASW; 100m thick),
168 extending from the Antarctic continental shelf to the PF, are characterised by near freezing temperatures and
169 salinity values up to 34.3 practical salinity units (PSU), although these properties can vary on a regional basis
170 (Carter et al., 2009 and references therein). The transition between AASW south of the PF and Sub-Antarctic
171 surface water (SASW) north of the SAF occurs in the Polar Frontal Zone. Due to complex mixing processes,

172 the properties of surface water in the Polar Frontal Zone are often variable, but this water is generally
173 warmer (3-8 °C) and less dense (salinity 34-34.4 PSU) than AASW (Carter et al., 2009 and references
174 therein). Lastly, SASW is comparatively warmer (6-12 °C) with salinity >34.3 PSU (Carter et al., 2009 and
175 references therein). Circumpolar Deep Water (CDW) together with CDW-derived, modified deep-water
176 masses, such as Warm Deep Water in the Weddell Gyre (e.g. Vernet et al., 2019) is a key Southern Ocean
177 water mass and can be detected between ~1400 m and >3500 m depth offshore from the Antarctic continent.
178 CDW can rise to meet AASW or even outcrop along the Antarctic continental margin (Carter et al., 2009 and
179 references therein). Mixing of CDW with different water masses gives rise to two types: Upper CDW
180 (UCDW) defined by an oxygen minimum, high nutrient concentrations, and a depth of 1400-2500 m; and
181 Lower CDW (LCDW) defined by a salinity maximum of 34.70-34.75 PSU (Carter et al., 2009 and
182 references therein). In contrast to UCDW, LCDW extends south of the SBACC (Orsi et al., 1995), is
183 upwelled at the continental slope, and can protrude onto the shelf where it mixes with shelf waters cooled by
184 interactions with the ice shelves and atmosphere (sometimes below the surface freezing point), renewing
185 LCDW and forming Antarctic Bottom Water (AABW) (Carter et al., 2009 and references therein).
186 The Scotia Sea is located in the eastern Atlantic sector of the Southern Ocean (20°W to 65°W) bounded by
187 the South Atlantic Ocean to the North, the Drake Passage to the West, and by the Weddell Sea to the South
188 (Figure 1). The Scotia Sea is influenced by the eastward flow of the ACC, via the Drake Passage, and by a
189 northward component of the ACC, caused by topographic steering and northward outflow of recently
190 ventilated waters from the Weddell Sea, whereby Weddell Sea Deep Water (WSDW) is incorporated into
191 the ACC (Locarnini et al., 1993; Naveira Garabato et al., 2002a,b), thus creating a region of high mixing
192 (Heywood et al., 2002) and intense water mass modification (Locarnini et al., 1993).
193 The Amundsen Sea extends from 100°W to 130°W and is bounded by the Sub-Antarctic Pacific to the North
194 (Figure 1). The Amundsen Sea water column south of the PF mainly consist of a thin upper layer of cold and
195 fresh AASW overlying relatively warm CDW. The Amundsen Sea Embayment is located offshore from one
196 of the major WAIS drainage basins and observations show a clear trend in glacial retreat over recent decades
197 (e.g. Mouginot et al., 2014; Paolo et al., 2015; Rignot et al., 2019). The deep ice shelves (extending up to
198 1000 m below sea level) surrounding the Amundsen Sea embayment are exposed to unmodified CDW which
199 can be up to 4 °C above the *in situ* freezing point (Jacobs et al., 1996, 2011; Rignot and Jacobs, 2002;

200 [Jenkins et al., 2010; Rignot et al., 2013; Webber et al., 2017](#)) so that CDW may drive enhanced melt rates
201 [and ice sheet instability in this region \(Shepherd et al., 2001; Zwally et al., 2005; Rignot et al., 2008;](#)
202 [Pritchard et al., 2009; Wingham et al., 2009\).](#)

203 [2.1.2.2.](#) **Sample collection**

204 A Seabird Scientific SBE911plus conductivity-temperature-depth (CTD) instrument with a 24 bottle rosette
205 was used to vertically profile the water column and collect water for organic geochemical analysis. Water
206 was collected on board the RRS *James Clark Ross* (expeditions JR272 and JR257) during March-April 2012
207 (austral autumn) from 15 stations along the former WOCE A23 section (Meredith et al., 2001) traversing the
208 Scotia Sea between the northern Weddell Sea and South Georgia (Table 1 and Figure 1; Allen et al., 2012;
209 Venables et al., 2012), and on board the R/V *Polarstern* expedition PS104 during February-March 2017
210 (austral summer) from 5 stations in the Amundsen Sea embayment (Table 2 and Figure 1; Gohl, 2017).
211 Water samples were collected in 10 L Niskin bottles. In the Scotia Sea, the depth of the sample collection
212 was dependent on the expression of the mixed layer and seasonal thermocline as observed during each CTD
213 deployment. At all stations, a “mixed layer” sample was collected between 10-40m depth and a “thermocline
214 layer” sample collected between approximately 60-110 m depth (Table 1). In the Amundsen Sea, the
215 sampling strategy included samples from surface thermocline waters, and CDW. Water samples
216 (approximately 10-30 L) were vacuum filtered through pre-combusted GF/F filters (Whatman, 0.7 µm pore
217 size, 50 mm diameter). Glass fibre filters with a nominal pore size of 0.7 µm are most commonly used for
218 sampling of SPM in ocean and lake waters. However, as microbes can range in size from 0.2-0.7 µm, these
219 filters may lead to an under-sampling of archaeal cells that are not associated with aggregates (Lee et al.,
220 1995; Ingalls et al., 2012). Therefore, IPL-GDGT concentrations reported here represent the minimum likely
221 concentrations.

222 The filters were subsequently stored in foil at -20 °C, then transported to Durham University (UK; Scotia sea
223 samples) and Alfred Wegener Institute (Germany; Amundsen Sea samples). Samples were freeze-dried prior
224 to lipid extraction.

225 [2.2.2.3.](#) **Sample extraction**

226 Total lipids of the Scotia Sea sample set were extracted at the Royal Netherlands Institute for Sea Research.
227 Freeze-dried samples were extracted using a modified Bligh and Dyer methodology as detailed in Besseling

228 et al. (2018). Briefly, sample filters were cut into small pieces using solvent cleaned scissors. The total lipids
229 were extracted using a monophasic mixture of K₂HPO₄ (8 g/L adjusted to pH 7-8), dichloromethane
230 (CH₂Cl₂) and methanol (CH₃OH) at a ratio of 0.8:1:2. Extractions were repeated three times and pooled. The
231 pooled extract was subsequently phase separated by adjusting the ratio of K₂HPO₄: CH₂Cl₂: CH₃OH to
232 0.9:1:1. The CH₂Cl₂ layer of the resultant bi-phasic mixture was transferred to a round bottom flask. This
233 was repeated three times, with the Bligh Dyer extract (~~BDE~~) dried under a stream of N₂.

234 Total lipids of the Amundsen Sea sample set were extracted at the Alfred Wegener Institute (Germany).
235 Freeze dried samples were extracted ultrasonically using CH₂Cl₂ and CH₃OH at a ratio of 2:1 for 15 minutes.
236 This was repeated three times, the extracts pooled and dried under a stream of N₂. The resulting total lipid
237 extract was fractionated over a silica column using hexane (for elution of the alkanes and highly branched
238 isoprenoids) followed by CH₂Cl₂:hexane and CH₂Cl₂:CH₃OH both at a ratio of 1:1 for elution of the polar
239 fraction. The polar fraction was dried under N₂ and stored at -20 °C prior to IPL-GDGT analysis. The
240 method used for the extraction of the Amundsen Sea samples is not the Bligh Dyer protocol most commonly
241 used for IPL-GDGT extraction. Extraction technique has not been found to significantly affect c-GDGTs
242 recovery (Schouten et al., 2013; Weber et al., 2017) but has been found to have a greater influence on IPL-
243 GDGT recovery due to differences in polar moieties (Weber et al., 2017). Weber et al. (2017) found
244 extraction procedure to impact the absolute quantification of GDGTs along with the recovery of cren'
245 (under-quantified) and GDGT-3 (over-quantified). Sample purification using silica gel column
246 chromatography has also been found to have an impact on IPL-GDGT recovery (Pitcher et al., 2009;
247 Lengger et al., 2012) with HPH-GDGTs under-quantified (Lengger et al., 2012). We acknowledge that there
248 may be some differences in IPL-GDGT recovery between the Amundsen and Scotia sea samples due to
249 differences in extraction and work-up technique. However, we propose that comparison can still be made
250 between the two seas as we do not report absolute quantities of IPL-GDGTs as the methods are semi-
251 quantitative, we do not report the occurrence of cren', and GDGT-3 was below the detection limit of the
252 instrument. The method used for the extraction of the Amundsen Sea samples is not the regular IPL
253 extraction procedure as it, for example, does not use phosphate buffer and that this may have an influence of
254 the results obtained for the Amundsen Sea samples.

255 An internal standard of 1-O-hexadecyl-2-acetyl-*sn*-glycero-3-phosphocholine was added to both the
256 Amundsen and Scotia Sea samples. The ~~TLE~~ Bligh Dyer extract (Scotia Sea) and polar fraction (Amundsen

257 Sea) were filtered through true regenerated cellulose filters (4 mm, 0.45 μm pore size) using hexane, propan-
258 2-ol, and water at a ratio of 79:20:1. Samples were stored at $-20\text{ }^{\circ}\text{C}$ prior to analysis.

259 2.3.2.4. Intact Polar Lipid characterisation

260 IPL-GDGTs were analysed using a modification of the Sturt et al. (2004) methodology as detailed in
261 Besseling et al. (2018). To summarise, an Agilent 1290 Infinity I UHPLC, equipped with a thermostated
262 auto-injector and column oven, coupled to a Q Exactive Orbitrap MS with Ion Max source with a heated
263 electrospray ionisation (HESI) probe (Thermo Fisher Scientific, Waltham, MA, USA). Separation was
264 achieved using a YMC-Triart Diol-HILIC column (250 x 2.0 mm, 1.9 μm particle size, 12 nm pore size;
265 YMC co., Ltd., Kyoto, Japan) maintained at $30\text{ }^{\circ}\text{C}$ with a flow rate of 0.2 mL/min. Chromatographic
266 separation of IPL-GDGTs was achieved using the following 70 minute program: 0% eluent B from 0-5
267 minutes, linear gradient to 34% eluent B at 25 minutes, isocratic 25-40 minutes, linear gradient to 60% B at
268 55 minutes, linear gradient to 70% B 65 minutes, followed by a re-equilibration time of 20 minutes between
269 each analysis. Eluent A was hexane/propan-2-ol/formic acid/ 14.8 M $\text{NH}_{3\text{aq}}$ (79:20:0.12:0.04 [v/v/v/v]),
270 eluent B is propan-2-ol/water/formic acid/14.8 M $\text{NH}_{3\text{aq}}$ (88:10:0.12:0.04 [v/v/v/v]). HESI sheath gas,
271 auxiliary gas and sweep gas N_2 pressures were 35, 10, and 10 (arbitrary units) respectively with the auxiliary
272 gas at $50\text{ }^{\circ}\text{C}$. The spray voltage was 4.0 kV (positive ion ESI), S-Lens 70 V, and capillary temperature 275
273 $^{\circ}\text{C}$. Mass range monitored was between m/z 375 and 2000 (resolving power of 70 000 ppm at m/z 200)
274 followed by data dependent fragmentation of the 10 most abundant masses in the mass spectrum (with the
275 exclusion of isotope peaks) were fragmented successively (stepped normalised collision energy 15, 22.5, 30;
276 isolation window 1.0 m/z). A dynamic exclusion window of 6 s was used as well as an inclusion list with a
277 mass tolerance of 3 ppm to target specific compounds (absolute m/z values of IPL-GDGTs can be found in
278 supplement A and structures are found in supplement B S1). The Q Exactive Orbitrap MS was calibrated
279 within a mass accuracy range of 1 ppm using the Thermo Scientific Pierce LTQ Velos ESI Positive Ion
280 Calibration Solution (containing a mixture of caffeine, MRFA, Ultramark 1621, and N-butylamine in an
281 acetonitrile-methanol-acetic acid solution). Peak areas for each individual IPL were determined by
282 integrating the combined mass chromatograms (within 3 ppm) of the monoisotopic and first isotope peak of
283 all the relevant adducts formed (protonated, ammoniated, and/or sodiated). IPL-GDGTs were examined in
284 terms of their MS peak area response. Thus, the relative abundance of the peak area does not necessarily

285 reflect the actual relative abundance of the different IPL-GDGTs, however, this method allows for the
286 comparison between samples analysed in this study. The peak areas were determined from extracted ion
287 chromatograms of the $[M+H]^+$, $[M+NH_4]^+$, and $[M+Na]^+$ for each individual IPL-GDGT species. C-GDGT
288 lipids were not analysed.

289 2.4.2.5. Data Analysis

290 Standards for individual IPL-GDGTs are not available and therefore; concentrations reported here are semi-
291 quantitative. IPL-GDGT peak areas were normalised to the internal standard and volume of water filtered
292 and are reported as units/L. The Ring Index (RI) was calculated based on Zhang et al. (2016).
293 Redundancy analysis (RDA) was performed on the Scotia Sea data set in RStudio (version 1.2.1335) using
294 Vegan and Faraway packages. RDA was performed using data normalised to the internal standard and total
295 water volume extracted (scaled). Temperature, salinity, oxygen concentration, and Chlorophyll A_a
296 fluorescence (hereafter referred to as fluorescence) were selected as explanatory variables and IPL-GDGT
297 relative abundances are the response variables. Statistical significance of RDA, axes, and explanatory
298 variables were determined using an Anova-like test (Legendre et al., 2011).

299 **3. Results**

300 **3.1. Physicochemical properties of the water column**

301 CTD measurements were taken at all 5 stations in the Amundsen Sea; PS104/003, PS104/007, PS104/017,
302 PS104/022, PS104/043. Temperature – salinity (T-S) plots are shown in Figure 2 and supplement B S2.
303 ~~Temperature, salinity, fluorescence, oxygen profiles are shown for each of the Amundsen Sea stations in~~
304 ~~Supplement B S1~~. At the time of sampling, water masses in the Amundsen Sea study area were characterised
305 by a temperature range of -1.7 to +1.1 °C, a salinity range of 32.8 to 34.7 PSU, and an dissolved oxygen
306 concentration of between 183.9-4.5 and 386.28-9 $\mu\text{molkgml/L}$ (Supplement B S1). ~~Ocean temperatures in the~~
307 ~~Amundsen Sea, generally show a relatively warm surface layer, followed by a steep thermocline to a~~
308 ~~temperature minimum (winter water) extending down to approximately 400m, with ocean temperatures~~
309 ~~increasing below this point due to the intrusion of relatively warm CDW (Supplement B S1)~~. Three different
310 water masses are detected in the Amundsen Sea from the T-S plot: AASW, CDW, and modified CDW
311 (Figure 2). Fluorescence peaked at the surface within the uppermost 20 m, followed by a steep decline with

312 depth (Supplement B S12). High fluorescence values were observed at PS104/017 with 8mg/m³, and
313 PS104/007 with 4 mg/m³ respectively, whereas low fluorescence values were observed at stations
314 PS104/003, PS104/022, and PS104/043 (Supplement B S12).
315 The Scotia Sea study area encompasses the SAF, PF, SACCF and the SBACC (Figure 1a) and is
316 characterised by a temperature range of -1.6 to +7.3 °C, and a salinity range of 33.6-34.7 PSU (Figure 2).
317 The temperature range of the mixed layer samples was -1.2 to +7.3 °C and thermocline samples was -1.6 to
318 +6.1 °C. A clear partition between the sample stations is observed in the T-S plot (Figure 2) with consistently
319 higher water temperatures found at stations north of CTD 19 and on average lower ocean temperatures south
320 of CTD 18. This region broadly marks the location of the SBACC at ~58.6 °S (Figure 1a).

321 **3.2. Intact Polar GDGT inventory**

322 ~~A total of 12 IPL GDGTs (see Supplement B S2 for structures) were identified within 48 samples from the~~
323 ~~Southern Ocean (Figure 3 and 4, Tables 3 and 4). This included IPLs with cores comprising of GDGT 0,~~
324 ~~GDGT 1, GDGT 2, cren, OH GDGTs 0, and diOH GDGT 0. It should be noted that the LC-MS method~~
325 ~~utilised in this study does not separate individual GDGT isomers, including crenarchaeol (cren) and its~~
326 ~~isomer, cren', and hence the cren detected here is likely a combination of both isomers. The majority of the~~
327 ~~IPL GDGTs in both the Amundsen and Scotia seas were regular GDGTs (i.e. not hydroxylated) with a mean~~
328 ~~contribution of 69% (±20%) and 66% (±18%) respectively (excluding samples where IPL GDGTs were~~
329 ~~absent). diOHGDGT 0 was the least common core lipid identified in the Scotia and Amundsen Sea. Both~~
330 ~~forms of hydroxyl GDGT were observed with zero cyclopentane moieties (OH GDGT 0 and diOH GDGT~~
331 ~~0). While GDGT 1, GDGT 2, and cren were detected, GDGT 0 was the dominant regular GDGT in both the~~
332 ~~Amundsen and Scotia seas. GDGT 0, cren, and OH GDGT 0 were all detected in combination with the MH,~~
333 ~~DH, and HPH head groups. GDGT 1 and GDGT 2 were only found to be associated with DH and diOH~~
334 ~~GDGT 0 was only found in combination with MH (Tables 2 and 3).~~

335 **3.3.3.2. Amundsen Sea depth profiles**

336 Archaeal IPLs were identified in the water column at all Amundsen Sea stations (Table 3, Figure 3). The
337 relative abundance of the regular GDGT core (i.e. non-hydroxylated) varied with depth ranging from 20-
338 100% of total IPL-GDGTs (excluding depths where no IPL-GDGTs were identified; Table 34). PS104/003

339 and PS104/007 were found to have IPL-GDGTs in the uppermost surface sample (10 m and 20 m depths
340 respectively). The surface sample at PS104/003 (10m) was dominated by non-hydroxylated GDGTs (94.3%
341 of total IPLs) with a lower relative abundance of OH-GDGT core type (5.7% of total IPLs). Further to this,
342 HPH-GDGT-0 was the most abundant IPL-GDGT at this station (81.8% of total IPLs) with HPH-cren
343 contributing a smaller fraction of the total IPL-GDGTs (11.1%). Low relative abundance of MH-GDGT-0
344 (<1%), MH-cren (<1%), MH-OH-GDGT-0 (<1%), DH-OH-GDGT-0 (5.1%), and MH-diOH-GDGT-0
345 (<1%) were also observed at PS104/003 10 m. This contrasts with the surface sample at PS104/007 (20 m)
346 where no OH-GDGT-IPLs were detected and where the IPL-GDGT suite is split between MH-GDGT-0
347 (89.1%) and MH-cren (10.9%). IPL-GDGTs were not identified within the surface sample at PS104/017 (10
348 m) and the two mid-shelf stations, PS104/022 (10 m and 30 m) and PS104/043 (10 m). DH-GDGT-0 and
349 DH-cren are minor components of the IPL-GDGT suite with maximum relative abundance observed in the
350 deepest samples for all Amundsen Sea stations. The relative abundance of IPL-GDGTs with a MH head
351 group peaks in the mid depths between 120 and 240 m (with the exception of the surface 20 m at
352 PS104/007). ~~Further to this, the ratio of MH/DH and MH/HPH is also highest at the mid depths between 120~~
353 ~~and 240 m (Table 5 and 6).~~ The ratio of GDGT-0/cren is variable throughout the Amundsen Sea stations,
354 ranging from 2.8-8.2 (excluding samples with no GDGTs). The sample taken from 180 m water depth at
355 PS104/003 exceeded this range with a GDGT-0/cren ratio of 27.0 (Table ~~25 and 6~~).

356 **3.4.3.3. Scotia Sea transect**

357 Archaeal IPLs were detected within all 16 Scotia Sea stations. A clear depth trend in IPL-GDGTs can be
358 observed where IPL-GDGTs were detected in the thermocline samples but were often below detection within
359 the mixed layer (Table 4 and Figure 4b). Exceptions to this are CTD 1, 16, 20, and 21 where IPL-GDGTs
360 were present in both the mixed and thermocline layers. Relative abundance (%) of IPL-GDGT cores and the
361 degree of cyclicity remains constant along the Scotia Sea transect with IPL-GDGT head groups showing
362 greater variation along the transect (Table 4). An increase in the relative abundance of the HPH head group is
363 observed within the thermocline samples between CTD 22 (53.5 °S) and 5 (63.3 °S) this is coupled with a
364 decrease in the relative abundance (%) of MH and DH IPL-GDGT head groups (Figure 43b). Mixed layer
365 CTD 20 and 21 are dominated by MH, CTD 16 is dominated by HPH, and CTD 1 mixed layer contains a
366 mixture of all three IPL-GDGT head groups. The GDGT-0/cren ratio generally ranges from 1.6-9.9, but CTD

367 7 (21.7), 10 (177.6), and 16 (16.8), located at the thermocline, exceed this range due to low cren
368 concentrations (Table 15). In preparation for RDA [on the thermocline samples](#), biomarkers that were
369 identified in fewer than three samples were designated “rare species” and were excluded from the analysis
370 (GDGT-DH-0, GDGT-DH-1 and OH-GDGT-HPH-0 excluded). This is because outliers can violate the
371 linearity of the relationship between the response and explanatory variables (Legendre & Legendre, 2012).
372 Samples [CTD 1](#) and 25 were also excluded from the analysis. [Sample-CTD 1](#) is located offshore of the
373 Falkland Islands and is the only sample from North of the SAF, thus representing the only data point for the
374 Subantarctic Zone of the Southern Ocean that is unlikely to be representative for the polar environment.
375 [Sample-CTD 25](#), located close to South Georgia, was excluded due to high biomarker abundances (Figure
376 [43a](#)) which could be due to exceptionally high productivity in this area (e.g. Atkinson et al., 2001). Variance
377 inflation factors (VIFs) for the response variables were between 3.5 (fluorescence) and 11.4 (oxygen
378 concentration) (Supplement C [Table 1](#)). The VIF for oxygen concentration is slightly higher than is typically
379 acceptable for RDA analysis. This is due to correlation between oxygen concentration and fluorescence
380 ($R_2=0.63$), however, as the R_2 is below 0.7 this is unlikely to violate the assumptions of the RDA (Legendre
381 & Legendre, 2012) ([Supplement C Table 2](#)). RDA shows 64% constrained variation with RDA1 and 2
382 accounting for 63% of the cumulative variation ([Supplement C Tables 3-5](#)). The RDA is statistically
383 significant ($p<0.05$, $f=3.5$), furthermore, RDA1 is found to be statistically significant ($p<0.05$, $f=11.48$)
384 however, RDA2 is not significant ($p=0.42$, $f=2.35$) ([Supplement C Tables 10-12](#)). Species scores show HPH-
385 GDGT-0 and HPH-cren to load positive on RDA 1, with MH-GDGT-0, MH-cren, MH-OH-GDGT-MH-0,
386 DH-OH-GDGT-0, and MH-MH-diOH-GDGT-0 loading highly negative on RDA1 ([Figure 5](#)). Of the
387 explanatory variables tested, temperature is statistically significant at the <0.05 level ($f=8.56$) and with
388 salinity ($p=0.07$, $f=2.61$) and oxygen concentration ($p=0.09$, $f=2.58$) approaching significance ([Supplement](#)
389 [C Table 12](#)). The site scores show CTD 20, 21, 22, 23, and 24 to be negatively loaded on RDA1 with CTD 3,
390 5, 7, 10, 13, 16, 18 and 19 to be positively loaded on RDA1 suggesting that these stations are contrasted
391 along this axis ([Figure 5](#)).

392 4. Discussion

393 4.1. Hydroxylated GDGTs in Polar Environments

394 In this study, two hydroxylated GDGTs (OH-GDGT-0 and diOH-GDGT-0) were detected. Hydroxylated
395 GDGTs have been reported as potential biomarkers for reconstructing ocean temperature change in cold
396 waters (Fietz et al., 2013, 2016) and in this study contribute up to 49.8% (OH-GDGT) and 30.1% (diOH-
397 GDGT) of total IPL-GDGTs. Hydroxylated IPL-GDGTs are not commonly reported in previous SPM
398 studies (e.g. Kim et al., 2016; Kang et al., 2017; Hurley et al., 2018). However, these compounds have been
399 reported as c-GDGTs in marine and lacustrine sediments, with hydroxylated GDGTs found to contribute
400 approximately 8% in marine sediments from temperate and tropical sites (Liu et al., 2012; Lu et al., 2015).
401 These compounds have been reported in much higher abundance in polar environments including up to 20%
402 in SPM and up to 16% in surface sediments from the Nordic Seas (Fietz et al., 2013) and up to 20% in
403 surface sediments from the Southern Ocean (Huguet et al., 2013).

404 ~~In the Amundsen and Scotia seas, hydroxylated GDGTs made up a significant amount of the total IPL-~~
405 ~~GDGT profile, contributing up to 79.9% (Amundsen Sea, PS104/003—180 m). Even excluding this one~~
406 ~~exceptional sample, hydroxylated IPL-GDGT abundances were still consistently above 20% with a~~
407 ~~maximum relative abundance of 48.1% in the Amundsen Sea and 68.5% of total IPL-GDGTs in the Scotia~~
408 ~~Sea (Table 3 and 4). Exceptionally high hydroxylated GDGT relative abundances of greater than 20% could~~
409 be due to differences in methodologies to the previous studies which measured core GDGTs by atmospheric
410 pressure chemical ionisation (APCI; Liu et al., 2012; Fietz et al., 2013; Huguet et al., 2013; Lu et al., 2015)
411 while this study examined IPL-GDGTs using electrospray ionisation (ESI). Using the same LC-MS
412 methodology, Sollai et al. (2019a) report average hydroxylated IPL-GDGT relative abundances of 22%
413 ($\pm 19\%$) with a range of 0-51% in SPM from the euxinic Black Sea; however, similar analyses from the
414 Arabian Sea (Besseling et al., 2018), the eastern tropical South Pacific (Sollai et al., 2019b) and the
415 Mediterranean Sea did not detect hydroxylated IPL-GDGTs. Molecular dynamics simulations have shown
416 that the addition of hydroxyl moieties in the tetraether structure increases the fluidity of the cell membrane
417 and aid trans-membrane transport in cold environments (Huguet et al., 2017). The exceptionally high amount
418 of hydroxylated IPL-GDGT for the Amundsen and Scotia seas may therefore be due to elevated synthesis of
419 these biomarkers in cold environments.

420 4.2. IPL-GDGT Distributions as an Indicator of Archaeal Populations

421 In both the Amundsen and Scotia Sea samples ~~GDGT-0 dominated the IPL-GDGT profiles contributing up~~
422 ~~to 89.1% of the total in the Amundsen Sea and up to 100% in the Scotia Sea.~~ Low diversity of cyclic
423 GDGTs ~~in this study~~ is observed indicated by (RI ranging from 0.02 – 1 for the Scotia Sea and 0.03 – 0.9 for
424 the Amundsen Sea; ~~(Tables 15 and 62)~~). This is particularly low compared with the RI of the global core top
425 calibration, which includes a range of Southern Ocean samples, reporting an RI range of 1.25-3 (excluding
426 the Red Sea samples; ~~)~~ (Kim et al., 2010; Ho et al., 2011, 2014; Zhang et al., 2016). Previous SPM studies
427 spanning a range of marine habitats have reported the presence of hydroxylated GDGT-1, -2, and -3 as well
428 as a wider range of non-hydroxylated GDGTs, such as GDGT-3 and -4 (Kim et al., 2016; Besseling et al.,
429 2018; Hurley et al., 2018; Sollai et al., 2019a,b). As this study used the same analytical methodology as
430 Besseling et al. (2018) and Sollai et al. (2019a,b), these differences cannot be attributed to analytical
431 methodologies. Low cyclic diversity of GDGTs in the Amundsen and Scotia seas could be due to differences
432 in the synthesis of these lipids by the source Thaumarchaeota. The relationship between ocean temperature
433 and the cyclicity of GDGTs has been firmly established, with increasing ocean temperatures correlated with
434 increasing relative abundance of GDGTs with 2 or more cyclopentane moieties (Schouten et al., 2002, 2007;
435 Kim et al., 2008, 2010). However, Kim et al. (2010) note some differences between sub-tropical and sub-
436 polar oceans, with cren playing a more important role in temperature reconstructions in the subtropics than in
437 polar oceans, suggesting that there may be differences in membrane adaptation strategies of
438 Thaumarchaeota. Principal component analysis of IPL-GDGT distributions of a moderately thermophilic
439 Thaumarchaeota along with previously published data identifies two distinct clusters with a clear partition
440 between the orders of Nitrosopumilales and Nitrososphaeales (Bale et al., 2019). IPL-GDGTs analysed in
441 this study cluster within the Nitrosopumilales group due to the high relative abundances of GDGT-0 and low
442 relative abundances of all other GDGTs. Due to the polar locations of the Amundsen and Scotia Sea samples,
443 Nitrosopumilales are likely to be the key AOA in these environments. Previous microbial analysis of the
444 spatial variation in prokaryotes of the Amundsen Sea polynya identified the most abundant Thaumarchaea
445 marine group I (MGI) sequence belonged to the cluster affiliated with “*Ca. Nitrosopumilus maritimus*” (Kim
446 et al., 2014). In similar studies within the wider Southern Ocean region phylogenetic analysis reveals high
447 abundances of sequences clustering with *Nitrosopumilus*. Hernandez et al. (2015) analysed surface water

448 samples from Potter Cove (King George Island, western Antarctica Peninsula) which revealed that the
449 majority of sequences fell into the clade containing “*Ca. Nitrosopumilus maritimus*” and other
450 environmental sequences containing Thaumarchaeota. Signori et al. (2018) studied microbial spatial and
451 temporal variability at 10 stations off the Antarctic peninsula revealing spring to be characterised by SAR11
452 and microbial communities remaining from winter, including Thaumarchaeota (*Nitrosopumilus*),
453 Euryarchaeota, and SAR324, with a shift in microbial populations during the summer and autumn.
454 Three polar head groups were detected in this study, i.e. MH, DH, and HPH. All three head groups have
455 previously been identified in culture (Schouten et al., 2008; Pitcher et al., 2011; Sinninghe Damsté et al.,
456 2012; Elling et al., 2017), environmental studies (e.g. Zhu et al., 2016; Besseling et al., 2018), and have
457 widely been associated with Thaumarchaeota. It has been postulated that specific IPL-GDGTs may be
458 associated with particular Thaumarchaeotal groups or habitats (Sinninghe Damsté et al., 2012; Elling et al.,
459 2017; Bale et al., 2019). Previously the HPH head group has been associated with the Nitrosopumilales order
460 (Group I.1a) and the DH head group with the Nitrososphaeales order (Group I.1b) (Sinninghe Damsté et al.,
461 2012). More recent studies have shown that environmental niche or habitat may be the main driver of GDGT
462 head group composition rather than phylogeny (Elling et al., 2017; Bale et al., 2019). Relevant to this study,
463 Elling et al. (2017) analysed the lipidome of 10 Thaumarchaeotal cultures and identified DH-GDGTs and DH-
464 OH-GDGTs as key membrane components of the marine mesophiles compared with the terrestrial
465 thermophilic and soil mesophilic Thaumarchaeota. In the present study, high abundances of HPH were
466 detected, contributing up to 92.9% and up to 100% of total IPL-GDGTs in the Amundsen Sea and Scotia Sea
467 respectively. The dominance of HPH in the lipid profiles of the Amundsen and Scotia seas align with
468 previous culture analysis (Schouten et al., 2008; Pitcher et al., 2011; Sinninghe Damsté et al., 2012; Elling et
469 al., 2017).

470 **4.3. Distribution of IPL-GDGTs in surface waters of Southern Ocean**

471 In this study, we observed a number of consistent trends in the water column IPL-GDGT distributions
472 between the different Amundsen Sea and Scotia Sea sampling stations. In the surface samples, collected
473 within the euphotic zone of the Amundsen Sea at PS104/017 (10 m), PS104/022 (10 m and 30 m),
474 PS104/043(10 m), and the Scotia sea (15-40m depth at CTD stations 3, 5, 7, 10, 13, 18, 19, 22, 23, 24, 25)
475 no IPL-GDGTs were identified. Previous studies from the Southern Ocean have shown water column

476 archaeal distributions to be highly variable on both a temporal and spatial scale. Broadly, archaea (as
477 measured by cell counts or rRNA) are often absent or found in relatively low abundance in the surface
478 waters during the austral spring algal bloom and during austral summer (Massana et al., 1998; Church et al.,
479 2003; Kalanetra et al., 2009; Besseling et al., 2020). The absence of archaea in the surface waters of the
480 Southern Ocean contrasts with the high abundance of bacteria and is part of a larger seasonal cycle in
481 archaeal population dynamics (Church et al., 2003). Temporal distributions of archaea are then shown to
482 become more evenly distributed by depth, with an increase in the population within the surface waters
483 throughout austral autumn-winter (Church et al., 2003). The Amundsen Sea samples were collected during
484 austral summer. Two previous studies in the Antarctic Peninsula have shown an increase in group I archaeal
485 populations in surface waters during austral summer and winter (Massana et al., 1998; Murray et al., 1998).
486 However, Kalanetra et al. (2009) did not observe any archaea in surface waters west of the Antarctic
487 Peninsula during austral summer. The mechanism for this temporal heterogeneity is likely mediated by a
488 combination of physical and biological factors including, water mass properties, concentrations of dissolved
489 and particulate organic carbon (Murray et al., 1998). Furthermore, the absence of AOA in the surface waters
490 during austral spring, when primary productivity is highest, could be due to competition with bacteria and
491 algae that bloom during the same time period and/or a subsequent nutrient limitation (Massana et al., 1998;
492 Church et al., 2003; Kalanetra et al., 2009). As the current study was only performed at one time point during
493 austral summer a larger sampling campaign would be required to fully characterise microbial and IPL-
494 GDGT seasonality in the Amundsen Sea.

495 In contrast with the other stations, the surface water samples from PS104/003 and PS104/007 (10 m and 20
496 m respectively) and CTD 1, 16, 20, and 21 were found to contain IPLs. The samples from PS104/007 (10 m),
497 CTD 20 and 21 only contained the MH head group. It should be noted that while the MH head group is
498 known to be synthesised by archaea (e.g. Sinninghe Damsté et al., 2012), this IPL is recalcitrant and can be
499 formed as a degradation product of other IPL-GDGTs (e.g. Lengger et al., 2013, 2014). In contrast, HPH is
500 more labile and less readily preserved in sediments following cell death and is hence considered to be a
501 biomarker for recently active archaea and, in particular, Thaumarchaeota (Pitcher et al., 2010; Sinninghe
502 Damsté et al., 2012). HPH-cren can vary between phylogenetic subgroups (Elling et al., 2017) and while DH
503 head group is not as labile as HPH due to its glycosidic structure (Lengger et al., 2013), DH-GDGTs have
504 been identified with consistent relative abundances across the Nitrosopumilales order (Group 1.1a).

505 suggesting DH-cren as an additional biomarker for AOA activity (Elling et al., 2017). Hence, the dominance
506 of the MH head group at these stations may indicate an inactive/relic archaeal population at this depth.
507 Higher IPL-GDGT diversity was detected at PS104/003 and CTD 1 and 16 including HPH and DH head
508 groups indicating a recently active archaeal population (Sinninghe Damsté et al., 2012; Elling et al., 2017).
509 PS104/003 is located in an area of active upwelling of nutrient-rich waters largely composed of CDW (Pine
510 Island Bay polynya) (Mankoff et al., 2012). Together with the Amundsen Polynya located north of Dotson
511 and westernmost Getz ice shelves (Figure 1), it is one of the most productive regions (per unit area) of the
512 Southern Ocean (Arrigo and van Dijken, 2003). Productivity is further aided by the influx of iron released
513 from the rapidly melting Thwaites and Pine Island glaciers (Alderkamp et al., 2012; Gerringa et al., 2012;
514 Thuroczy et al., 2012; St-Laurent et al., 2017). Results from another cruise in the region identified that
515 productivity is limited not only by nutrient and iron availability but also by light; productivity is 30-50%
516 lower in the Pine Island Polynya compared to the Amundsen Polynya, with this difference attributed to the
517 significant difference in solar irradiance levels between the two polynyas throughout the summer season
518 (Park et al., 2017). Similarly, CTD 1 is located close to the Falkland Islands in the Subantarctic Zone north
519 of the SAF and is potentially subject to additional terrestrial inputs and coastal dynamics. Kalanetra et al.
520 (2009) suggests that a combination of both light and nutrient differences between Arctic and Antarctic ocean
521 settings could cause the differences in archaeal populations in the surface ocean, where low light and nutrient
522 levels in the surface allows archaeal populations to flourish, with further studies suggesting photoinhibition
523 of Thaumarchaeota (Church et al., 2003; Mincer et al., 2007; Hu et al., 2011; Merbt et al., 2012; Luo et al.,
524 2014).
525 Results show IPL GDGTs to be absent from the mixed layer samples (15-40 m). Samples were collected
526 between March and April 2012 and, similar to the Amundsen Sea, the absence of IPL GDGTs at these
527 stations could be due to photo-inhibition and competition from bacteria and algae at the surface (Church et
528 al., 2003; Mincer et al., 2007; Hu et al., 2011; Merbt et al., 2012; Luo et al., 2014). IPL GDGTs are present
529 at the surface CTD 1, 21, 20, and 16. CTD 21 and 20 are dominated by MH, which implies relic and not
530 active archaeal populations (Lengger et al., 2013, 2014). CTD 16 contains low relative abundances of HPH-
531 GDGT-0 which could indicate some archaeal activity. However, CTD 1 contains greater IPL diversity
532 including DH and HPH head groups potentially suggesting a recently active archaeal community at the

533 surface. CTD 1 is located close to the Falkland Islands in the Subantarctic Zone north of the SAF and is
534 potentially subject to additional terrestrial inputs and coastal dynamics.

535 **4.3.4.4. Influence of Circumpolar Deep Water on IPL Distributions: Amundsen Sea**

536 ~~In this study, we observed a number of consistent trends in the water column IPL-GDGT distributions~~
537 ~~between the different Amundsen Sea sampling stations. In the surface samples, collected within the euphotic~~
538 ~~zone at PS104/017 (10 m), PS104/022 (10 m and 30 m), PS104/043(10 m), no IPL-GDGTs were identified.~~
539 ~~Previous studies from the Southern Ocean have shown water column archaeal distributions to be highly~~
540 ~~variable on both a temporal and spatial scale. Broadly, archaea (as measured by cell counts or rRNA) are~~
541 ~~often absent or found in relatively low abundance in the surface waters during the austral spring algal bloom~~
542 ~~and during austral summer (Massana et al., 1998; Church et al., 2003; Kalanetra et al., 2009; Besseling et al.,~~
543 ~~2020). The absence of archaea in the surface waters of the Southern Ocean contrasts with the high abundance~~
544 ~~of bacteria and is part of a larger seasonal cycle in archaeal population dynamics (Church et al., 2003).~~
545 ~~Temporal distributions of archaea are then shown to become more evenly distributed by depth, with an~~
546 ~~increase in the population within the surface waters throughout austral autumn-winter (Church et al., 2003).~~
547 ~~The Amundsen Sea samples were collected during austral summer. Two previous studies in the Antarctic~~
548 ~~Peninsula show an increase in group I archaeal populations in surface waters during austral summer and~~
549 ~~winter (Massana et al., 1998; Murray et al., 1998). However, Kalanetra et al. (2009) did not observe any~~
550 ~~archaea in surface waters west of the Antarctic Peninsula during austral summer. The mechanism for this~~
551 ~~temporal heterogeneity is likely mediated by a combination of physical and biological factors including,~~
552 ~~water mass properties, concentrations of dissolved and particulate organic carbon (Murray et al., 1998).~~
553 ~~Furthermore, the absence of AOA in the surface waters during austral spring, when primary productivity is~~
554 ~~highest, could be due to competition with bacteria and algae that bloom during the same time period and/or a~~
555 ~~subsequent nutrient limitation (Massana et al., 1998; Church et al., 2003; Kalanetra et al., 2009). As the~~
556 ~~current study was only performed at one time point during austral summer a larger sampling campaign~~
557 ~~would be required to fully characterise microbial and IPL-GDGT seasonality in the Amundsen Sea.~~
558 ~~In contrast to the other stations, the surface water samples from PS104/003 and PS104/007 (10 m and 20 m~~
559 ~~respectively) were found to contain IPLs. Unusually, the samples from PS104/007 (10 m) only contained the~~
560 ~~MH head group. It should be noted that while the MH head group is known to be synthesised by archaea~~

561 (e.g. Sinninghe Damsté et al., 2012), this IPL is recalcitrant and can be formed as a degradation product of
562 other IPL-GDGTs (e.g. Lengger et al., 2013, 2014). In contrast, HPH is more labile and less readily
563 preserved in sediments following cell death and is hence considered to be a biomarker for recently active
564 archaea and, in particular, Thaumarchaeota (Pitcher et al., 2010; Sinninghe Damsté et al., 2012). While DH
565 head group is not as labile as HPH due to its glycosidic structure (Lengger et al., 2013), the prevalence of
566 DH across the Thaumarchaeota phylum may suggest some use of this head group as a biomarker for the
567 archaeal community (Elling et al., 2017). Hence, the dominance of the MH head group at this station may
568 indicate an inactive/relic archaeal population at this depth. Higher IPL-GDGT diversity was detected at
569 PS104/003 including HPH and DH head groups indicating a recently active archaeal population (Sinninghe
570 Damsté et al., 2012; Elling et al., 2017). PS104/003 is located in an area of active upwelling of nutrient rich
571 waters largely composed of CDW (Pine Island Bay polynya) (Mankoff et al., 2012). Together with the
572 Amundsen Polynya located north of Dotson and westernmost Getz ice shelves (Figure 1), it is one of the
573 most productive regions (per unit area) of the Southern Ocean (Arrigo and van Dijken, 2003). Productivity is
574 further aided by the influx of iron released from the rapidly melting Thwaites and Pine Island glaciers
575 (Alderkamp et al., 2012; Gerringa et al., 2012; Thuroczy et al., 2012; St Laurent et al., 2017). Productivity in
576 this area is not only limited by nutrient and iron availability but also by light; productivity is 30-50% lower
577 in the Pine Island Polynya compared to the Amundsen Polynya, with this difference attributed to the
578 significant difference in solar irradiance levels between the two polynyas throughout the summer season
579 (Park et al., 2017). Kalanetra et al. (2009) suggests that a combination of both light and nutrient differences
580 between Arctic and Antarctic ocean settings could cause the differences in archaeal populations in the
581 surface ocean, where low light and nutrient levels in the surface allows archaeal populations to flourish, with
582 further studies suggesting photoinhibition of Thaumarchaeota (Church et al., 2003; Mincer et al., 2007; Hu et
583 al., 2011; Merbt et al., 2012; Luo et al., 2014).

584 IPL-GDGT diversity increased downwards in the water column through the thermocline and the CDW layer
585 in the Amundsen Sea (Figure Table 34). DH-cren and HPH-cren may be widely applied as biomarkers for
586 recently active Thaumarchaeota populations having been identified as key cell membrane lipids (Pitcher et
587 al., 2010; Sinninghe Damsté et al., 2012; Elling et al., 2017). HPH-cren was identified consistently
588 throughout the thermocline and CDW layer at all Amundsen Sea stations (Table 34). Our results, therefore,
589 suggest recently active AOA at the thermocline and within the CDW. Tolar et al. (2016) shows ammonia

590 oxidation (AO) to occur throughout the water column, with similar rates of AO in CDW during both winter
591 and summer seasons and increased AO in surface waters during the late winter in sites west of the Antarctic
592 Peninsula. ~~These patterns in AO are is-~~consistent with molecular microbiology studies from the Amundsen
593 Sea and Antarctic Peninsula region that identified~~y~~ Thaumarchaeota throughout the water column, but with a
594 seasonal trend where these archaea are often absent in the surface waters during spring and summer, and
595 present in the CDW throughout the ~~season-year~~(Massana et al., 1998; Alonso-Saez et al., 2011). HPH-cren,
596 however, may not be the most suitable proxy for tracking the complete AOA population as the relative
597 abundance of this IPL can vary significantly between phylogenetic subgroups (Elling et al., 2017). DH-
598 GDGTs have been identified with consistent relative abundances across the Nitrosopumilales order (Group
599 1.1a), suggesting DH-cren as an additional biomarker for AOA activity (Elling et al., 2017). In this study we
600 detect DH-cren consistently in the CDW layer and with low relative abundance in the thermocline of
601 PS104/003 and PS104/007 and absence in the thermocline waters at PS104/017 and PS104/022.

602 Thaumarchaeota are thought to partition between shallow water (0-130 m) and deep water (500-4000 m)
603 marine clades (Francis et al., 2005; Hallam et al., 2006). Therefore, ~~this difference in the depth trend of~~
604 HPH-cren ~~throughout the thermocline and CDW~~ and DH-cren ~~restricted to CDW depths-distributions~~ could
605 reflect differences in Thaumarchaeota populations in the Amundsen Sea. While the data presented here
606 provide only a snapshot of the Amundsen Sea IPL-GDGT distributions, this small contrast in HPH and DH-
607 cren distributions may represent a significant partition between Thaumarchaeota populations and warrants
608 further analysis. ~~Thaumarchaeota are not homogeneously distributed throughout the water column.~~
609 ~~Molecular microbiology has identified Thaumarchaeota to be virtually absent from Antarctic Summer~~
610 ~~Surface Waters (0-45m depth) and present in Winter Water (45-105m depth) and Circumpolar Deep Water~~
611 ~~(105-3500m depth) (e.g. Kalanetra et al., 2009). Our observation of active IPL-GDGT synthesis within the~~
612 ~~CDW has implications for the use of c-GDGT based biomarker proxies in the Amundsen Sea and potentially~~
613 ~~more broadly within the Southern Ocean. Indeed, temperature reconstructions based on GDGTs are~~
614 ~~suggested to represent the 45-200m range (Kim et al., 2012), acknowledging the absence of Thaumarchaeota~~
615 ~~from the surface waters during the summer months in Antarctica. The influence of CDW on reconstructed~~
616 ~~TEX₈₆ paleo temperatures has been hypothesised in Adélie Land (East Antarctica) with Kim et al. (2012)~~
617 ~~suggesting warmer reconstructed temperatures were likely due to the upwelling of CDW onto the piston core~~
618 ~~site. In our study we specifically observe IPL-GDGTs of recently living archaea in the CDW (over 500 m~~

619 water depth). Furthermore, we observe a shift in head group composition at CDW depths in the Amundsen
620 sea representing a shift in the IPL-GDGT producing community. We hypothesise that the contribution of
621 GDGTs synthesised at CDW depths where physical parameters (e.g. temperature) can be strikingly different
622 to the 45-200m water depth may have a significant impact on reconstructed TEX₈₆ temperatures, not only the
623 Amundsen Sea but potentially more broadly within the Southern Ocean.

624 **4.4.4.5. Influences on the GDGT-IPL distribution along the Scotia Sea Transect**

625 ~~Samples from the Scotia Sea were taken along a transect spanning 54 °S—64 °S (Figure 1a). The T-S plot~~
626 ~~(Figure 2) shows the CTD profiles for stations taken along the transect between 64 °S and 58.6 °S (CTD 3-~~
627 ~~21) located south of the SBACC and stations between 53 °S and 58.6 °S (CTD 1, 22-25) located in the~~
628 ~~Antarctic zone between the SBACC and the PF (Figure 1a). Results show IPL-GDGTs to be absent from the~~
629 ~~mixed layer samples (15-40 m). Samples were collected between March and April 2012 and, similar to the~~
630 ~~Amundsen Sea, the absence of IPL-GDGTs at these stations could be due to photo-inhibition and~~
631 ~~competition from bacteria and algae at the surface (Church et al., 2003; Mincer et al., 2007; Hu et al., 2011;~~
632 ~~Merbt et al., 2012; Luo et al., 2014). IPL-GDGTs are present at the surface CTD 1, 21, 20, and 16. CTD 21~~
633 ~~and 20 are dominated by MH, which implies relic and not active archaeal populations (Lengger et al., 2013,~~
634 ~~2014). CTD 16 contains low relative abundances of HPH-GDGT 0 which could indicate some archaeal~~
635 ~~activity. However, CTD 1 contains greater IPL diversity including DH and HPH head groups potentially~~
636 ~~suggesting a recently active archaeal community at the surface. CTD 1 is located close to the Falkland~~
637 ~~Islands in the Subantarctic Zone north of the SAF and is potentially subject to additional terrestrial inputs~~
638 ~~and coastal dynamics.~~

639 IPL-GDGTs were ~~also~~ found to be present within the thermocline (60-110 m) and contain a high proportion
640 of MH head group IPL-GDGTs, suggesting a high proportion of relic IPL-GDGTs in the Scotia Sea that
641 could relate to variability in the seasonality of archaeal populations. Further to this, DH-cren was found to be
642 absent from the thermocline, with HPH-cren intermittently present. This pattern in DH-cren and HPH-cren in
643 the Scotia Sea ~~This~~ is consistent with our results from the Amundsen Sea where DH-cren was mostly absent
644 from the 120-240m depth intervals but present in the CDW depth intervals (i.e. below 400m), while HPH-
645 cren was present at both the thermocline and CDW depths.

646 ~~As noted above, the~~The Scotia Sea samples were collected along clear temperature (-1.6 to +7.3 °C), salinity
647 (33.6 -34.3 PSU), oxygen (218.3-332.7 $\mu\text{mol/kg m}^{-1}$), and fluorescence (0.03-1.1 $\text{ml}^{-1}\text{m}^{-3}$) gradients
648 associated with ocean fronts, which are known to impact bacterioplankton population diversity (Wilkins et
649 al., 2013; Baltar et al., 2016; Raes et al., 2018). Figure 5 shows that higher latitude samples with cooler
650 ocean temperatures cluster positively on RDA axis 1 and have higher relative abundances of HPH-GDGT-0
651 and HPH-cren (samples 3, 5, 7, 10, 13, 16, 18, 19), whilst samples from warmer ocean waters and lower
652 latitudes cluster negatively on RDA axis 1 and have higher relative abundances of MH and DH IPL-GDGTs
653 (samples 20 – 24). ~~The contrast in IPL headgroup distributions between CTD stations 3-19 and 20-24 is~~
654 suggests that RDA 1 represents the transition across the SBACC. Temperature was found to be statistically
655 significant explanatory variable in the RDA which is consistent with previous research that has identified
656 clear links between core GDGT relative abundances and environmental variables such as temperature
657 (Schouten et al., 2007; Kim et al., 2008, 2010). Specifically, we observe a shift in the GDGT head group
658 between the warmer and cooler waters of the ACC fronts. Temperature, along with other physicochemical
659 properties (e.g. nutrient and oxygen concentrations) vary across the ACC (e.g. Rubin, 2003; Freeman et al.,
660 2019). These shifts in physicochemical properties across permanent oceanic boundaries influence and control
661 bacterial and archaeal species richness, creating ecological boundaries or niches (e.g. Raes et al., 2018).
662 Variability in IPL-GDGT headgroup composition observed across the Scotia Sea transect could reflect the
663 transition across an environmental niche (e.g. Elling et al., 2017; Bale et al., 2019). As this study is limited
664 by the number of chemical properties analysed, it would be speculative to infer the relative importance of
665 specific nutrient concentrations across the Scotia Sea transect.

666 Alternatively, the shift in IPL-GDGT head group could also be influenced by the presence of the Weddell
667 Gyre which is located south of 55-60 °S, and between 60 °W and 30 °E (~~Deacon et al., 1979~~Vernet et al.,
668 2019). The Weddell Gyre is a region of enhanced productivity, with austral summer chlorophyll *A-a*
669 concentrations ranging from 1.5-10 $\mu\text{g/L mg m}^{-3}$ (Bathmann et al., 1997; Cape et al. 2014) due to high
670 concentrations of nutrients upwelled and circulated through the gyre (Vernet et al., 2019 and references
671 therein).

672 5. Conclusions

673 A range of archaeal IPLs ~~were~~ detected in both the Amundsen Sea and the Scotia Sea. High relative
674 abundances of OH-GDGT core type were observed which could reflect the polar environmental setting of
675 these samples. Low cyclicity was detected in both the Amundsen and Scotia Seas for both the GDGT and
676 OH-GDGT core type with acyclic OH-GDGT-0 and GDGT-0, -1, -2, and cren reported. Low cyclicity of
677 GDGTs may potentially be a more widespread feature of the Southern Ocean GDGT signature.
678 IPL-GDGT relative abundance along the Scotia Sea transect shows a distinct pattern across the
679 oceanographic front transition. Samples south of the SBACC and from cooler ocean waters had higher
680 relative abundances of HPH-GDGT-0 and HPH-cren compared with samples north of the SBACC, and while
681 those from warmer ocean waters had higher relative abundances of MH and DH IPL-GDGTs. Indeed, RDA
682 reveals that temperature is a significant explanatory variable, however, productivity and nutrient availability
683 may also play a role in IPL-GDGT distributions. Additionally, this shift in IPL-GDGT distributions could
684 represent a shift in the dominant archaeal IPL synthesisers and/or a physiological survival strategy.
685 In the Amundsen Sea ~~a high relative abundance of IPL-GDGTs are detected~~ throughout the water column ~~is~~
686 ~~indicative of Thaumarchaeota activity both within the thermocline and CDW.~~ IPL-GDGTs of recently living
687 archaea were specifically observed in the CDW (over 500 m water depth) along with a shift in head group
688 composition at CDW depths representing a shift in the IPL-GDGT producing community. We hypothesise
689 that the contribution of GDGTs synthesised at CDW depths where physical parameters, such as temperature,
690 can be strikingly different to the upper water column (e.g. 0-200m water depth) may have a significant
691 impact on reconstructed TEX₈₆^L temperatures in not only the Amundsen sea but potentially more broadly
692 within the Southern Ocean. Indeed, the Thaumarchaeotal populations within CDW could make a significant
693 GDGT contribution to the sedimentary record which could have implications for GDGT-based temperature
694 reconstructions.
695 ~~IPL-GDGT relative abundance along the Scotia Sea transect shows a distinct pattern across the~~
696 ~~oceanographic front transition. Samples south of the SBACC and from cooler ocean waters having higher~~
697 ~~relative abundances of HPH-GDGT-0 and HPH-cren compared with samples north of the SBACC, and from~~
698 ~~warmer ocean waters having higher relative abundances of MH and DH IPL-GDGTs. Indeed RDA reveals~~
699 ~~that temperature is a significant explanatory variable, however, productivity and nutrient availability may~~

700 ~~also play a role in IPL-GDGT distributions. Additionally, this shift in IPL-GDGT distributions could~~
701 ~~represent a shift in the dominant archaeal IPL synthesisers and/or a physiological survival strategy.~~

702

703 Data availability

704 CTD data from JR257/JR272A are available from the British Oceanographic Data Centre at

705 <https://www.bodc.ac.uk/data/documents/cruise/11431/>.

706 Author contributions

707 CSJ, ELM, CDH, EM, JAS designed the experiments. CSJ, NJB, ECH, JM undertook the laboratory

708 preparation and analysis. EPAPV, CA, TB, VP generated the oceanographic data. CSJ and AS undertook

709 statistical analysis. CSJ, ELM, NJB, ECH, SS, JAS wrote the manuscript with contributions from all authors.

710 Competing interests

711 The authors declare that they have no conflicting interests.

712 Acknowledgments

713 This project was funded through a UK Natural Environment Research Council (NERC) Standard Grant,

714 awarded to JS, ELM, CDH, and Kate Hendry (NE/M013081/1), a British Antarctic Survey Collaborative

715 Gearing Scheme award (ELM), a Helmholtz Research Grant (VH-NG-1101; JM), and the Durham

716 University Department of Geography Research Development Fund (CSJ). N.B. is funded by the European

717 Research Council (ERC) under the European Union's Horizon 2020 research and innovation program (grant

718 agreement no.694569). Collection of CTD casts on the A23 transect was supported by NERC National

719 Capability funding to BAS. We thank M.D. West, A.J. Hayton, and D. Dorhout for technical support. -We

720 are grateful to the captains, crews, support staff and scientists participating in cruises JR257, JR272 and

721 PS104, and acknowledge funding for cruise PS104 by AWI, MARUM, BAS and NERC UK-IODP. Lastly,

722 we thank two anonymous reviewers for their constructive comments that improved the manuscript.

723 6. References

724 Alderkamp, A.-C., Mills, M. M., van Dijken, G. L., Laan, P., Thuroczy, C.-E., Gerringa, L. J. A., de Baar, H.

725 J. W., Payne, C. D., Visser, R. J. W., Buma, A. G. J. and Arrigo, K. R.: Iron from melting glaciers fuels

726 phytoplankton blooms in the Amundsen Sea (Southern Ocean): Phytoplankton characteristics and

727 productivity, Deep-Sea Res. Part II- Top. Stud. Oceanogr., 71–76, 32–48,
728 <https://doi.org/10.1016/j.dsr2.2012.03.005>, 2012.

729 Allen, C. S., Peck, V. L., Graham, A. G. C., Blagbrough, H., Robinson, M. W. and McClymont, E.: RRS
730 James Clark Ross Marine Science Cruises JR257 and JR254e, March-April 2012, British Antarctic Survey,
731 Cambridge, UK, https://www.bodc.ac.uk/resources/inventories/cruise_inventory/reports/jr257_254e.pdf,
732 2012.

733 Alonso-Saez, L., Sanchez, O., Gasol, J. M., Balague, V. and Pedros-Alio, C.: Winter-to-summer changes in
734 the composition and single-cell activity of near-surface Arctic prokaryotes, Environ. Microbiol., 10, 2444–
735 2454, <https://doi.org/10.1111/j.1462-2920.2008.01674.x>, 2008.

736 Alonso-Saez, L., Andersson, A., Heinrich, F. and Bertilsson, S.: High archaeal diversity in Antarctic
737 circumpolar deep waters, Environ. Microbiol. Rep., 3, 689–697, [https://doi.org/10.1111/j.1758-](https://doi.org/10.1111/j.1758-2229.2011.00282.x)
738 [2229.2011.00282.x](https://doi.org/10.1111/j.1758-2229.2011.00282.x), 2011.

739 Arrigo, K. and van Dijken, G.: Phytoplankton dynamics within 37 Antarctic coastal polynya systems, J.
740 Geophys. Res. – Oceans., 108, <https://doi.org/10.1029/2002JC001739>, 2003.

741 Atkinson, A., Whitehouse, M.J., Priddle, J., Cripps, G.C., Ward, P. and Brandon, M.A.: South Georgia,
742 Antarctic: a productive, cold water, pelagic ecosystem, Mar.Ecol.Prog.Ser., 216, 279-308,
743 <https://doi.org/10.3354/meps216279>, 2001.

744 Bale, N.J., Palatinszky, M., Rijpstra, W.I.C., Herbold, C.W., Wagner, M., Sinninghe Damsté, J.S.:
745 Membrane lipid composition of the moderately thermophilic ammonia-oxidising archaeon “*Candidatus*
746 *Nitrosotenuis uzonensis*” at different growth temperatures. Appl. Environ. Microbiol.,85, [https://doi.org/](https://doi.org/10.1128/AEM.01332-19)
747 [10.1128/AEM.01332-19](https://doi.org/10.1128/AEM.01332-19), 2019.

748 Baltar, F., Currie, K., Stuck, E., Roosa, S. and Morales, S. E.: Oceanic fronts: transition zones for
749 bacterioplankton community composition, Environ. Microbiol. Rep., 8, 132–138,
750 <https://doi.org/10.1111/1758-2229.12362>, 2016.

751 Bathmann, U.V., Scharek, R., Klaas, C., Dubischar, C.D. and Smetacek, V.: Spring development of
752 phytoplankton biomass and composition in major water masses of the Atlantic sector of the Southern Ocean,

753 Deep Sea Res. Part II Top. Stud. Oceanogr. 44, 51-67, [https://doi.org/10.1016/S0967-0645\(96\)00063-X](https://doi.org/10.1016/S0967-0645(96)00063-X),
754 1997.

755 Bauersachs, T., Speelman, E. N., Hopmans, E. C., Reichart, G. J., Schouten, S. and Sinninghe Damsté, J. S.:
756 Fossilized glycolipids reveal past oceanic N₂ fixation by heterocystous cyanobacteria, Proc. Natl. Acad. Sci.
757 U. S. A., 107, 19190–19194, <https://doi.org/10.1073/pnas.1007526107>, 2010.

758 Besseling, M. A., Hopmans, E. C., Boschman, R. C., Sinninghe Damsté, J. S. and Villanueva, L.: Benthic
759 archaea as potential sources of tetraether membrane lipids in sediments across an oxygen minimum zone,
760 Biogeosciences, 15, 4047–4064, <https://doi.org/10.5194/bg-15-4047-2018>, 2018.

761 Besseling, M. A., Hopmans, E. C., Bale, N. J., Schouten, S., Sinninghe Damsté, J. S. and Villanueva, L.: The
762 absence of intact polar lipid-derived GDGTs in marine waters dominated by Marine Group II: Implications
763 for lipid biosynthesis in Archaea. Sci. Rep., 10, <https://doi.org/10.1038/s41598-019-57035-0>, 2020.

764 Brochier-Armanet, C., Boussau, B., Gribaldo, S. and Forterre, P.: Mesophilic crenarchaeota: proposal for a
765 third archaeal phylum, the Thaumarchaeota, Nat. Rev. Microbiol., 6, 245–252,
766 <https://doi.org/10.1038/nrmicro1852>, 2008.

767 Cape, M.R., Vernet, M., Kahru, M. and Spreen, G.: Polynya dynamics drive primary production in the
768 Larsen A and B embayments following ice shelf collapse, J. Geophys. Res. Oceans, 119, 572-594,
769 <https://doi.org/10.1002/2013JC009441>, 2014.

770 Carter, L., McCave, I. N. and Williams, M. J. M.: Circulation and water masses of the Southern Ocean: A
771 Review, Antarct. Clim. Evol., 8, 85–114, [https://doi.org/10.1016/S1571-9197\(08\)00004-9](https://doi.org/10.1016/S1571-9197(08)00004-9), 2009.

772 Church, M. J., DeLong, E. F., Ducklow, H. W., Karner, M. B., Preston, C. M. and Karl, D. M.: Abundance
773 and distribution of planktonic Archaea and Bacteria in the waters west of the Antarctic Peninsula, Limnol.
774 Oceanogr., 48, 1893–1902, <https://doi.org/10.4319/lo.2003.48.5.1893>, 2003.

775 Darfeuil, S., Menot, G., Giraud, X., Rostek, F., Tachikaea, K., Garcia, M. and Bard, E.: Sea surface
776 temperature reconstructions over the last 70 kyr off Portugal: Biomarker data and regional modelling,
777 Paleoceanogr. Paleoclimatol. 31, 40-65, <https://doi.org/10.1002/2015PA002831>, 2016.

778 ~~Deacon, G. E. R.: The Weddell gyre, Deep Sea Res. Part I Oceanogr. Res. Pap., 26, 981-995,~~
779 ~~[https://doi.org/10.1016/0198-0149\(79\)90044-X](https://doi.org/10.1016/0198-0149(79)90044-X), 1979.~~

780 Delong, E. F., Wu, K. Y., Prezelin, B. B. and Jovine, R. V. M.: High abundance of archaea in Antarctic
781 marine picoplankton, *Nature*, 371, 695–697, <https://doi.org/10.1038/371695a0>, 1994.

782 Elling, F. J., Konneke, M., Lipp, J. S., Becker, K. W., Gagen, E. J. and Hinrichs, K. U.: Effects of growth
783 phase on the membrane lipid composition of the thaumarchaeon *Nitrosopumilus maritimus* and their
784 implications for archaeal lipid distributions in the marine environment, *Geochim. Cosmochim. Acta*, 141,
785 579–597, <https://doi.org/10.1016/j.gca.2014.07.005>, 2014.

786 Elling, F. J., Konneke, M., Nicol, G. W., Stieglmeier, M., Bayer, B., Spieck, E., de la Torre, J. R., Becker, K.
787 W., Thomm, M., Prosser, J. I., Herndl, G. J., Schleper, C. and Hinrichs, K. U.: Chemotaxonomic
788 characterisation of the Thaumarchaeal lipidome, *Environ. Microbiol.*, 19, 2681–2700,
789 <https://doi.org/10.1111/1462-2920.13759>, 2017.

790 Etourneau, J., Collins, L. G., Willmott, V., Kim, J. H., Barbara, L., Leventer, A., Schouten, S., Sinninghe
791 Damsté, J. S., Bianchini, A., Klein, V., Crosta, X. and Massé, G.: Holocene climate variations in the western
792 Antarctic Peninsula: evidence for sea ice extent predominantly controlled by changes in insolation and
793 ENSO variability, *Clim. Past*, 9, 1431–1446, <https://doi.org/10.5194/cp-9-1431-2013>, 2013.

794 Etourneau, J., Sgubin, G., Crosta, X., Swingedouw, D., Willmott, V., Barbara, L., Houssais, M-N., Schouten,
795 S., Sinninghe Damsté, J.S., Goosse, H., Escutia, C., Crespin, J., Massé, G. and Kim, J-H.: Ocean temperature
796 impact on ice shelf extent in the eastern Antarctic Peninsula, *Nat. Commun.* 10, 1-8,
797 <https://doi.org/10.1038/s41467-018-08195-6>, 2019.

798 Evans, T. W., Wormer, L., Lever, M. A., Lipp, J. S., Lagostina, L., Lin, Y. S., Jorgensen, B. B. and Hinrichs,
799 K. U.: Size and composition of subseafloor microbial community in the Benguela upwelling area examined
800 from intact membrane lipid and DNA analysis, *Org. Geochem.*, 111, 86–100,
801 <https://doi.org/10.1016/j.orggeochem.2017.06.008>, 2017.

802 Fietz, S., Huguet, C., Rueda, G., Hambach, B. and Rosell-Melé, A.: Hydroxylated isoprenoidal GDGTs in
803 the Nordic Seas, *Mar. Chem.*, 152, 1–10, <https://doi.org/10.1016/j.marchem.2013.02.007>, 2013.

804 Fietz, S., Ho, S. L., Huguet, C., Rosell-Mele, A. and Martinez-Garcia, A.: Appraising GDGT-based seawater
805 temperature indices in the Southern Ocean, *Org. Geochem.*, 102, 93–105,
806 <https://doi.org/10.1016/j.orggeochem.2016.10.003>, 2016.

807 Francis, C. A., Roberts, K. J., Beman, J. M., Santoro, A. E. and Oakley, B. B.: Ubiquity and diversity of
808 ammonia-oxidizing archaea in water columns and sediments of the ocean, *Proc. Natl. Acad. Sci. U. S. A.*,
809 102, 14683–14688, <https://doi.org/10.1073/pnas.0506625102>, 2005.

810 Freeman, N. M., Munro, D. R., Sprintall, J., Mazloff, M. R., Purkey, S., Rosso, I., DeRanek, C. A. and
811 Sweeney, C.: The observed seasonal cycle of macronutrients in Drake Passage: Relationship to fronts and
812 utility as a model metric, *J. Geophys. Res. Oceans*, 124, 4763–4783, <https://doi.org/10.1029/2019JC015052>,
813 2019.

814 Gerringa, L. J. A., Alderkamp, A.-C., Laan, P., Thuroczy, C.-E., De Baar, H. J. W., Mills, M. M., van
815 Dijken, G. L., van Haren, H. and Arrigo, K. R.: Iron from melting glaciers fuels the phytoplankton blooms in
816 Amundsen Sea (Southern Ocean): Iron biogeochemistry, *Deep-Sea Res. Part II- Top. Stud. Oceanogr.*, 71–
817 76, 16–31, <https://doi.org/10.1016/j.dsr2.2012.03.007>, 2012.

818 Gohl, K.: The Expedition PS104 of the Research Vessel POLARSTERN to the Amundsen Sea in 2017,
819 Alfred-Wegener-Institut, Helmholtz-Zentrum für Polar- und Meeresforschung, Bremerhaven, Germany,
820 https://doi.org/10.2312/BzPM_0712_2017, 2017.

821 Hallam, S. J., Mincer, T. J., Schleper, C., Preston, C. M., Roberts, K., Richardson, P. M. and DeLong, E. F.:
822 Pathways of carbon assimilation and ammonia oxidation suggested by environmental genomic analyses of
823 marine Crenarchaeota, *Plos Biol.*, 4, 520–536, <https://doi.org/10.1371/journal.pbio.0040095>, 2006.

824 Hernandez, E.A., Piquet, A.M.T., Lopez, J.L., Buma, A.G.J. and Mac Cormack, W.P.: Marine archaeal
825 community structure from Potter Cove, Antarctica: high temporal and spatial dominance of the phylum
826 Thaumarchaeota, *Polar. Biol.*, 38, 117-130, <https://doi.org/10.1007/s00300-014-1569-8>, 2015

827 Heywood, K. J., [Naveira](#) Garabato, A. C. ~~N.~~ and Stevens, D. P.: High mixing rates in the abyssal Southern
828 Ocean, *Nature*, 415, 1011–1014, <https://doi.org/10.1038/4151011a>, 2002.

829 Hillenbrand, C.-D., Smith, J.A., Hodell, D.A., Greaves, M., Poole, C.R., Kender, S., Williams, M.,
830 Andersen, T.J., Jernas, P.E., Elderfield, H., Klages, J.P., Roberts, S.J., Gohl, K., Larter, R.D. and Kuhn, G.:
831 West Antarctic Ice Sheet retreat driven by Holocene warm water incursions, *Nature* 547, 43-48
832 <https://doi.org/10.1038/nature22995>, 2017.

833 Ho, S. L., Mollenhauer, G., Feitz, S., Martinez-Garcia, A., Lamy, F., Rueda, G., Schipper, K., Méheust, M.,
834 Rosell-Melé, Stein, R. and Tiedemann, R.: Appraisal of TEX86 and TEX86L thermometries in subpolar and
835 polar regions, *Geochim. Cosmochim. Acta.*, 131, 213-226, [https://doi.org/ 10.1016/j.gca.2014.01.001](https://doi.org/10.1016/j.gca.2014.01.001), 2014.

836 Ho, S. L., Yamamoto, M., Mollenhauer, G. and Minagawa, M.: Core top TEX86 values in the South and
837 equatorial Pacific, *Org. Geochem.*, 42, 94-99, [https://doi.org/ 10.1016/j.orggeochem.2010.10.012](https://doi.org/10.1016/j.orggeochem.2010.10.012), 2011.

838 Hu, A. Y., Jiao, N. Z., Zhang, R. and Yang, Z.: Niche partitioning of marine group I Crenarchaeota in the
839 euphotic and upper mesopelagic zones of the East China Sea, *Appl. Environ. Microbiol.*, 77, 7469–7478,
840 <https://doi.org/10.1128/Aem.00294-11>, 2011.

841 Huguet, C. Kim, J.-H., Sinninghe Damsté, J.S. and Schouten, S.: Reconstruction of sea surface temperature
842 variations in the Arabian Sea over the last 23 kyr using organic proxies (TEX86 and U37K'), *Paleoceanogr.*
843 *Paleoclimatol.*, 21, PA3003, <https://doi.org/10.1029/2005PA001215>, 2006.

844 Huguet, C., Urakawa, H., Martens-Habbena, W., Truxal, L., Stahl, D. A. and Ingalls, A. E.: Changes in intact
845 membrane lipid content of archaeal cells as an indication of metabolic status, *Org. Geochem.*, 41, 930–934,
846 <https://doi.org/10.1016/j.orggeochem.2010.04.012>, 2010.

847 Huguet, C., Martrat, B., Grimalt, J.O., Sinninghe Damsté, J.S. and Schouten, S.: Coherent millennial-scale
848 patterns in U37k' and TEX86H temperature records during the penultimate interglacial-to-glacial cycle in the
849 western Mediterranean, 26, PA2218, [https://doi.org/ 10.1029/2010PA002048](https://doi.org/10.1029/2010PA002048), 2011.

850 Huguet, C., Fietz, S. and Rosell-Melé, A.: Global distribution patterns of hydroxy glycerol dialkyl glycerol
851 tetraethers, *Org. Geochem.*, 57, 107–118, <https://doi.org/10.1016/j.orggeochem.2013.01.010>, 2013.

852 Huguet, C., Fietz, S., Rosell-Mele, A., Daura, X. and Costenaro, L.: Molecular dynamics simulation study of
853 the effect of glycerol dialkyl glycerol tetraether hydroxylation on membrane thermostability, *Biochim.*
854 *Biophys. Acta-Biomembr.*, 1859, 966–974, <https://doi.org/10.1016/j.bbamem.2017.02.009>, 2017.

855 Hurley, S. J., Lipp, J. S., Close, H. G., Hinrichs, K. U. and Pearson, A.: Distribution and export of isoprenoid
856 tetraether lipids in suspended particulate matter from the water column of the Western Atlantic Ocean, *Org.*
857 *Geochem.*, 116, 90–102, <https://doi.org/10.1016/j.orggeochem.2017.11.010>, 2018.

858 Ingalls, A. E., Shah, S. R., Hansman, R. L., Aluwihare, L. I., Santos, G. H., Druffel, E. R. M. and Pearson,
859 A.: Quantifying archaeal community autotrophy in the mesopelagic ocean using natural radiocarbon, PNAS,
860 103, 6442-6447, [https://doi.org/ 10.1073/pnas.0510157103](https://doi.org/10.1073/pnas.0510157103), 2006.

861 Ingalls, A. E., Huguet, C. and Truxal, L.: Distribution of Intact and Core Membrane Lipids of Archaeal
862 Glycerol Dialkyl Glycerol Tetraethers among Size-Fractionated Particulate Organic Matter in Hood Canal,
863 Puget Sound, Appl. Environ. Microbiol., 78, 1480-1490, [https://doi.org/ 10.1128/AEM.07016-11](https://doi.org/10.1128/AEM.07016-11), 2012.

864 Jacobs, S. S., Hellmer, H. H. and Jenkins, A.: Antarctic ice sheet melting in the Southeast Pacific, Geophys.
865 Res. Lett., 23, 957-960, <https://doi.org/10.1029/96gl00723>, 1996.

866 Jacobs, S. S., Jenkins, A., Giulivi, C. F. and Dutrieux, P.: Stronger ocean circulation and increased melting
867 under Pine Island Glacier ice shelf, Nat. Geosci., 4, 519-523, <https://doi.org/10.1038/ngeo1188>, 2011.

868 Jenkins, A., Dutrieux, P., Jacobs, S. S., McPhail, S. D., Perrett, J. R., Webb, A. T. and White, D.:
869 Observations beneath Pine Island Glacier in West Antarctica and implications for its retreat, Nat. Geosci., 3,
870 468-472, <https://doi.org/10.1038/ngeo890>, 2010.

871 Jenkyns, H.C., Forster, A., Schouten, S. and Sinninghe Damsté, J.S.: High temperatures in the Late
872 Cretaceous Arctic Ocean, Nature, 432, 888-892, [https://doi.org/ 10.1038/nature03143](https://doi.org/10.1038/nature03143), 2004.

873 Joughin, I., Smith, B. E. and Medley, B.: Marine ice sheet collapse potentially under way for the Thwaites
874 Glacier Basin, West Antarctica, Science, 344, 735-738, <https://doi.org/10.1126/science.1249055>, 2014.

875 Kalanetra, K. M., Bano, N. and Hollibaugh, J. T.: Ammonia-oxidizing archaea in the Arctic Ocean and
876 Antarctic coastal waters, Environ. Microbiol., 11, 2434-2445, <https://doi.org/10.1111/j.1462->
877 2920.2009.01974.x, 2009.

878 Kang, S. J., Shin, K. H. and Kim, J. H.: Occurrence and distribution of hydroxylated isoprenoid glycerol
879 dialkyl glycerol tetraethers (OH-GDGTs) in the Han River system, South Korea, Acta Geochim., 36, 367-
880 369, <https://doi.org/10.1007/s11631-017-0165-3>, 2017.

881 Kim, J.-G., Park, S.-J., Quan, Z.-X., Jung, M.-Y., Cha, I.-T., Kim, S.-J., Kim, K.-H., Yang, E.-J., Kim, Y.-N.,
882 Lee, S.-H. and Rhee, S.-K.: Unveiling abundance and distribution of planktonic bacteria and archaea in a
883 polynya in Amundsen Sea, Antarctica, Environ. Microbiol., 16, 1566-1578, [https://doi.org/ 10.1111/1462-](https://doi.org/10.1111/1462-)
884 2920.12287. 2014.

885 Kim, J. -H., Schouten, S., Hopmans, E. C., Donner, B. and Sinninghe Damsté, J. S.: Global sediment core-
886 top calibration of the TEX86 paleothermometer in the ocean, *Geochim. Cosmochim. Acta*, 72, 1154–1173,
887 <https://doi.org/10.1016/i.gca.2007.12.010>, 2008.

888 Kim, J. -H., van der Meer, J., Schouten, S., Helmke, P., Willmott, V., Sangiorgi, F., Koç, N., Hopmans, E. C.
889 and Sinninghe Damsté, J. S.: New indices and calibrations derived from the distribution of crenarchaeal
890 isoprenoid tetraether lipids: Implications for past sea surface temperature reconstructions, *Geochim.*
891 *Cosmochim. Acta*, 74, 4639–4654, <https://doi.org/10.1016/j.gca.2010.05.027>, 2010.

892 Kim, J.-H., Crosta, X., Willmott, V., Renssen, H., Bonnin, J., Helmke, P., Schouten, S. and Sinninghe
893 Damsté, J. S.: Holocene subsurface temperature variability in the eastern Antarctic continental margin,
894 *Geophys. Res. Lett.*, 39, n/a-n/a, <https://doi.org/10.1029/2012gl051157>, 2012.

895 Kim, J.-H., Villanueva, L., Zell, C. and Sinninghe Damsté, J. S.: Biological source and provenance of deep-
896 water derived isoprenoid tetraether lipids along the Portuguese continental margin, *Geochim. Cosmochim.*
897 *Acta*, 172, 177–204, <https://doi.org/10.1016/j.gca.2015.09.010>, 2016.

898 Kirchman, D. L., Elifantz, H., Dittel, A. I., Malmstrom, R. R. and Cottrell, M. T.: Standing stocks and
899 activity of Archaea and Bacteria in the western Arctic Ocean, *Limnol. Oceanogr.*, 52, 495–507,
900 <https://doi.org/10.4319/lo.2007.52.2.0495>, 2007.

901 Lee, S. H., Kang, Y-C. and Fuhrman, J. A.: Imperfect retention of natural bacterioplankton cells by glass
902 fiber filters, *Mar. Ecol. Prog. Ser.*, 119, 285-290, <https://doi.org/10.3354/meps119285>, 1995.

903 Legendre, P., Oksanen, J. and ter Braak, C.J.: Testing the significance of canonical axes in redundancy
904 analysis, *Methods Ecol. Evol.*, 2, 269-277, <https://doi.org/10.1111/j.2041-210X.2010.00078.x>, 2011.

905 Legendre, P. and Legendre, L.: *Numerical Ecology*, Third Edition, Elsevier, Oxford (UK), ISBN: 978-0-444-
906 53869-7, 2012.

907 [Lengger, S.K., Hopmans, E.C., Sinninghe Damsté, J.S. & Schouten, S.: Comparison of extraction and work](#)
908 [up techniques for analysis of core and intact polar tetraether lipids from sedimentary environments. *Org.*](#)
909 [*Geochem.* 47, 34-40, <http://doi.org/10.1016/j.orggeochem.2012.02.009>, 2012.](#)

910 Lengger, S. K., Kraaij, M., Tjallingii, R., Baas, M., Stuut, J.-B., Hopmans, E. C., Sinninghe Damsté, J. S.
911 and Schouten, S.: Differential degradation of intact polar and core glycerol dialkyl glycerol tetraether lipids

912 upon post-depositional oxidation, *Org. Geochem.*, 65, 83–93,
913 <https://doi.org/https://doi.org/10.1016/j.orggeochem.2013.10.004>, 2013.

914 Lengger, S. K., Hopmans, E. C., Sinninghe Damsté, J. S. and Schouten, S.: Fossilization and degradation of
915 archaeal intact polar tetraether lipids in deeply buried marine sediments (Peru Margin), *Geobiology*, 12, 212–
916 220, <https://doi.org/10.1111/gbi.12081>, 2014.

917 Lincoln, S. A., Wai, B., Eppley, J. M., Church, M. J., Summons, R. E. and DeLong, E. F.: Planktonic
918 Euryarchaeota are a significant source of archaeal tetraether lipids in the ocean, *Proc. Natl. Acad. Sci. U. S.*
919 *A.*, 111, 9858–9863, <https://doi.org/10.1073/pnas.1409439111>, 2014a.

920 Lincoln, S. A., Wai, B., Eppley, J. M., Church, M. J., Summons, R. E. and DeLong, E. F.: Reply to Schouten
921 et al.: Marine Group II planktonic Euryarchaeota are significant contributors to tetraether lipids in the ocean,
922 *Proc. Natl. Acad. Sci. U. S. A.*, 111, E4286–E4286, <https://doi.org/10.1073/pnas.1416736111>, 2014b.

923 Lipp, J. S. and Hinrichs, K. U.: Structural diversity and fate of intact polar lipids in marine sediments,
924 *Geochim. Cosmochim. Acta*, 73, 6816–6833, <https://doi.org/10.1016/j.gca.2009.08.003>, 2009.

925 Lipp, J. S., Morono, Y., Inagaki, F. and Hinrichs, K. U.: Significant contribution of Archaea to extant
926 biomass in marine subsurface sediments, *Nature*, 454, 991–994, <https://doi.org/10.1038/nature07174>, 2008.

927 Liu, X. L., Lipp, J. S., Simpson, J. H., Lin, Y. S., Summons, R. E. and Hinrichs, K. U.: Mono- and
928 dihydroxyl glycerol dibiphytanyl glycerol tetraethers in marine sediments: Identification of both core and
929 intact polar lipid forms, *Geochim. Cosmochim. Acta*, 89, 102–115,
930 <https://doi.org/10.1016/j.gca.2012.04.053>, 2012.

931 Locarnini, R. A., Whitworth, T. and Nowlin, W. D.: The importance of the Scotia Sea on the outflow of
932 Weddell Sea Deep-Water, *J. Mar. Res.*, 51, 135–153, <https://doi.org/10.1357/0022240933223846>, 1993.

933 Lu, X. X., Liu, X. L., Elling, F. J., Yang, H., Xie, S. C., Song, J. M., Li, X. G., Yuan, H. M., Li, N. and
934 Hinrichs, K. U.: Hydroxylated isoprenoid GDGTs in Chinese coastal seas and their potential as a
935 paleotemperature proxy for mid-to-low latitude marginal seas, *Org. Geochem.*, 89–90, 31–43,
936 <https://doi.org/10.1016/j.orggeochem.2015.10.004>, 2015.

937 Luo, H. W., Tolar, B. B., Swan, B. K., Zhang, C. L. L., Stepanauskas, R., Moran, M. A. and Hollibaugh, J.
938 T.: Single-cell genomics shedding light on marine Thaumarchaeota diversification, *Isme J.*, 8, 732–736,
939 <https://doi.org/10.1038/ismej.2013.202>, 2014.

940 Mankoff, K. D., Jacobs, S. S., Tulaczyk, S. M. and Stammerjohn, S. E.: The role of Pine Island Glacier ice
941 shelf basal channels in deep-water upwelling, polynyas and ocean circulation in Pine Island Bay, Antarctica,
942 *Ann. Glaciol.*, 53, 123–128, <https://doi.org/10.3189/2012AoG60A062>, 2012.

943 Massana, R., Taylor, L. J., Murray, A. E., Wu, K. Y., Jeffrey, W. H. and DeLong, E. F.: Vertical distribution
944 and temporal variation of marine planktonic archaea in the Gerlache Strait, Antarctica, during early spring,
945 *Limnol. Oceanogr.*, 43, 607–617, <https://doi.org/10.4319/lo.1998.43.4.0607>, 1998.

946 Menviel, L., Timmermann, A., Timm, O. E. and Mouchet, A.: Climate and biogeochemical response to a
947 rapid melting of the West Antarctic Ice Sheet during interglacials and implications for future climate,
948 *Paleoceanography*, 25, <https://doi.org/10.1029/2009PA001892>, 2010.

949 Merbt, S. N., Stahl, D. A., Casamayor, E. O., Marti, E., Nicol, G. W. and Prosser, J. I.: Differential
950 photoinhibition of bacterial and archaeal ammonia oxidation, *Fems Microbiol. Lett.*, 327, 41–46,
951 <https://doi.org/10.1111/j.1574-6968.2011.02457.x>, 2012.

952 Meredith, M. P., Naveira Garabato, A. C., Stevens, D. P., Heywood, K. J., and Sanders, R. J.: Deep and
953 Bottom Waters in the Eastern Scotia Sea: Rapid Changes in Properties and Circulation, *J. Phys. Oceanogr.*,
954 31, 2157–2168, [https://doi.org/10.1175/1520-0485\(2001\)031<2157:DABWIT>2.0.CO;2](https://doi.org/10.1175/1520-0485(2001)031<2157:DABWIT>2.0.CO;2), 2001.

955 Mincer, T. J., Church, M. J., Taylor, L. T., Preston, C., Kar, D. M. and DeLong, E. F.: Quantitative
956 distribution of presumptive archaeal and bacterial nitrifiers in Monterey Bay and the North Pacific
957 Subtropical Gyre, *Environ. Microbiol.*, 9, 1162–1175, <https://doi.org/10.1111/j.1462-2920.2007.01239.x>,
958 2007.

959 Mougnot, J., Rignot, E. and Scheuchl, B.: Sustained increase in ice discharge from the Amundsen Sea
960 Embayment, West Antarctica, from 1973 to 2013, *Geophys. Res. Lett.*, 41, 1576–1584, <https://doi.org/10.1002/2013GL059069>, 2014.

962 Murray, A. E., Preston, C. M., Massana, R., Taylor, L. T., Blakis, A., Wu, K. and DeLong, E. F.: Seasonal
963 and spatial variability of bacterial and archaeal assemblages in the coastal waters near Anvers Island,
964 Antarctica, Appl. Environ. Microbiol., 64, 2585–2595, [https://doi.org/ 10.1128/AEM.64.7.2585-2595](https://doi.org/10.1128/AEM.64.7.2585-2595), 1998.

965 Naveira Garabato, A. C., Heywood, K. J. and Stevens, D. P.: Modification and pathways of Southern Ocean
966 Deep Waters in the Scotia Sea, Deep Sea Res. Part I Oceanogr. Res. Pap., 49, 681-705, [https://doi.org/
967 10.1016/S0967-0637\(01\)00071-1](https://doi.org/10.1016/S0967-0637(01)00071-1), 2002a.

968 Naveira Garabato, A. C., Strass, V. H. and Kattner, G.: Fluxes of nutrients in a three-dimensional meander
969 structure of the Antarctic Polar Front, Deep Sea Res. Part II Top. Stud. Oceanogr., 49, 3771-3792,
970 [https://doi.org/10.1016/S0967-0645\(02\)00110-8](https://doi.org/10.1016/S0967-0645(02)00110-8), 2002b.

971 Orsi, A. H., Whitworth, T. and Nowlin Jr., W. D.: On the meridional extent and fronts of the Antarctic
972 Circumpolar Current, Deep Sea Res. Part I Oceanogr. Res. Pap., 42, 641-673, [https://doi.org/10.1016/0967-
973 0637\(95\)00021-W](https://doi.org/10.1016/0967-0637(95)00021-W), 1995.

974 Paolo, F. S., Fricker, H. A. and Padman, L.: Volume loss from Antarctic ice shelves is accelerating, Science,
975 348, 327-331, <https://doi.org/10.1126/science.aaa0940>, 2015.

976 Park, J., Kuzminov, F. I., Bailleul, B., Yang, E. J., Lee, S., Falkowski, P. G. and Gorbunov, M. Y.: Light
977 availability rather than Fe controls the magnitude of massive phytoplankton bloom in the Amundsen Sea
978 polynyas, Antarctica, Limnol. Oceanogr., 62, 2260–2276, <https://doi.org/10.1002/lno.10565>, 2017.

979 [Pitcher, A., Hopmans, E.C., Schouten, S. & Sinninghe Damste, J.S.: Separation of core and intact polar
980 archaeal tetraether lipids using silica columns: Insights into living and fossil biomass contributions, Org.
981 Geochem. 40, 12-19, <http://doi.org/10.1016/j.orggeochem.2008.09.008>, 2009.](https://doi.org/10.1016/j.orggeochem.2008.09.008)

982 Pitcher, A., Rychlik, N., Hopmans, E. C., Spieck, E., Rijpstra, W. I. C., Ossebaar, J., Schouten, S., Wagner,
983 M. and Sinninghe Damsté, J. S.: Crenarchaeol dominates the membrane lipids of “*Candidatus*
984 *Nitrososphaera gargensis*”, a thermophilic Group I. 1b Archaeon, Isme J., 4, 542–552,
985 <https://doi.org/10.1038/ismej.2009.138>, 2010.

986 Pitcher, A., Hopmans, E. C., Mosier, A. C., Park, S. J., Rhee, S. K., Francis, C. A., Schouten, S. and
987 Sinninghe Damsté, J. S.: Core and Intact Polar Glycerol Dibiphytanyl Glycerol Tetraether Lipids of

988 Ammonia-Oxidizing Archaea Enriched from Marine and Estuarine Sediments, *Appl. Environ. Microbiol.*,
989 77, 3468–3477, <https://doi.org/10.1128/Aem.02758-10>, 2011.

990 Pritchard, H. D., Arthern, R. J., Vaughan, D. G. and Edwards, L. A.: Extensive dynamic thinning on the
991 margins of the Greenland and Antarctic ice sheets, *Nature*, 461, 971–975,
992 <https://doi.org/10.1038/nature08471>, 2009.

993 Raes, E. J., Bodrossy, L., van de Kamp, J., Bissett, A., Ostrowski, M., Brown, M. V., Sow, S. L. S., Sloyan,
994 B. and Waite, A. M.: Oceanographic boundaries constrain microbial diversity gradients in the South Pacific
995 Ocean, *Proc. Natl. Acad. Sci.*, 115, E8266–E8275, <https://doi.org/10.1073/pnas.1719335115>, 2018.

996 Raiswell, R., Benning, L. G., Tranter, M. and Tulaczyk, S.: Bioavailable iron in the Southern Ocean: the
997 significance of the iceberg conveyor belt, *Geochem. Trans.*, 9, <https://doi.org/10.1186/1467-4866-9-7>, 2008.

998 Rignot, E. and Jacobs, S. S.: Rapid bottom melting widespread near Antarctic ice sheet grounding lines,
999 *Science*, 296, 2020–2023, <https://doi.org/10.1126/science.1070942>, 2002.

1000 Rignot, E., Bamber, J. L., Van Den Broeke, M. R., Davis, C., Li, Y. H., Van De Berg, W. J. and Van
1001 Meijgaard, E.: Recent Antarctic ice mass loss from radar interferometry and regional climate modelling, *Nat.*
1002 *Geosci.*, 1, 106–110, <https://doi.org/10.1038/ngeo102>, 2008.

1003 Rignot, E., Jacobs, S., Mouginot, J. and Scheuchl, B.: Ice-Shelf Melting Around Antarctica, *Science*, 341,
1004 266–270, <https://doi.org/10.1126/science.1235798>, 2013.

1005 Rignot, E., Mouginot, J., Scheuchl, B., Van Den Broeke, M., Van Wessem, M.J. and Morlighem, M.: Four
1006 decades of Antarctic ice sheet mass balance from 1979-2017, *PNAS*, 116, 1095-1103, [https://doi.org/](https://doi.org/10.1073/pnas.1812883116)
1007 [10.1073/pnas.1812883116](https://doi.org/10.1073/pnas.1812883116), 2019.

1008 Rubin, S. I.: Carbon and nutrient cycling in the upper water column across the Polar Frontal Zone and
1009 Antarctic Circumpolar Current along 170°W, *Glob. Biogeochem. Cycles*, 17, 1-14,
1010 <https://doi.org/10.1029/2002GB001900>, 2003.

1011 Schouten, S., Hopmans, E. C., Pancost, R. D. and Sinninghe Damsté, J. S.: Widespread occurrence of
1012 structurally diverse tetraether membrane lipids: Evidence for the ubiquitous presence of low-temperature
1013 relatives of hyperthermophiles, *Proc. Natl. Acad. Sci. U. S. A.*, 97, 14421–14426,
1014 <https://doi.org/10.1073/pnas.97.26.14421>, 2000.

1015 Schouten, S., Hopmans, E. C., Schefuß, E. and Sinninghe Damsté, J. S.: Distributional variations in marine
1016 crenarchaeotal membrane lipids: a new tool for reconstructing ancient sea water temperatures?, *Earth Planet.*
1017 *Sci. Lett.*, 204, 265–274, [https://doi.org/10.1016/S0012-821X\(02\)00979-2](https://doi.org/10.1016/S0012-821X(02)00979-2), 2002.

1018 [Schouten, S., Hopmans, E.C., Rosell-Melé, A., Pearson, A., Adam, P., Bauersachs, T., Bard, E., Bernasconi,](#)
1019 [S.M., Bianchi, T.S., Brocks, J.J., Carlson, L.T., Castañeda, I.S., Derenne, S., Selver, A.D., Dutta, K.,](#)
1020 [Eglinton, T., Fosse, C., Galy, V., Grice, K., Hinrichs, K.U., Huang, Y., Huguet, A., Huguet, C., Hurley, S.,](#)
1021 [Ingalls, A., Jia, G., Keely, B., Knappy, C., Kondo, M., Krishnan, S., Lincoln, S., Lipp, J., Mangelsdorf, K.,](#)
1022 [Martínez-García, A., Ménot, G., Mets, A., Mollenhauer, G., Ohkouchi, N., Ossebaar, J., Pagani, M., Pancost,](#)
1023 [R.D., Pearson, E.J., Peterse, F., Reichart, G.J., Schaeffer, P., Schmitt, G., Schwark, L., Shah, S.R., Smith,](#)
1024 [R.W., Smittenberg, R.H., Summons, R.E., Takano, Y., Talbot, H.M., Taylor, K.W.R., Tarozo, R., Uchida,](#)
1025 [M., Van Dongen, B.E., Van Mooy, B.A.S., Wang, J., Warren, C., Weijers, J.W.H., Werne, J.P., Woltering,](#)
1026 [M., Xie, S., Yamamoto, M., Yang, H., Zhang, C.L., Zhang, Y., Zhao, M. & Sinninghe Damsté, J.S.: An](#)
1027 [interlaboratory study of TEX86 and BIT analysis of sediments, extracts, and standard mixtures, *Geochem.*](#)
1028 [*Geophys. Geosyst.*, 14, 5263-5265, <https://doi.org/10.1002/2013GC004904>, 2013.](#)

1029 Schouten, S., Huguet, C., Hopmans, E. C., Kienhuis, M. V. M. and Sinninghe Damsté, J. S.: Analytical
1030 methodology for TEX86 paleothermometry by high-performance liquid chromatography/atmospheric
1031 pressure chemical ionization-mass spectrometry, *Anal. Chem.*, 79, 2940–2944,
1032 <https://doi.org/10.1021/ac062339v>, 2007.

1033 Schouten, S., Baas, M., Hopmans, E. C., Reysenbach, A. L. and Sinninghe Damsté, J. S.: Tetraether
1034 membrane lipids of Candidatus “*Aciduliprofundum boonei*”, a cultivated obligate thermoacidophilic
1035 euryarchaeote from deep-sea hydrothermal vents, *Extremophiles*, 12, 119–124,
1036 <https://doi.org/10.1007/s00792-007-0111-0>, 2008.

1037 Schouten, S., Middelburg, J. J., Hopmans, E. C. and Sinninghe Damsté, J. S.: Fossilization and degradation
1038 of intact polar lipids in deep subsurface sediments: A theoretical approach, *Geochim. Cosmochim. Acta*, 74,
1039 3806–3814, <https://doi.org/10.1016/j.gca.2010.03.029>, 2010.

1040 Schouten, S., Pitcher, A., Hopmans, E. C., Villanueva, L., van Bleijswijk, J. and Sinninghe Damsté, J. S.:
1041 Intact polar and core glycerol dibiphytanyl glycerol tetraether lipids in the Arabian Sea oxygen minimum

1042 zone: I. Selective preservation and degradation in the water column and consequences for the TEX86,
1043 *Geochim. Cosmochim. Acta*, 98, 228–243, <https://doi.org/10.1016/j.gca.2012.05.002>, 2012.

1044 Schouten, S., Hopmans, E. C. and Sinninghe Damsté, J. S.: The organic geochemistry of glycerol dialkyl
1045 glycerol tetraether lipids: A review, *Org. Geochem.*, 54, 19–61,
1046 <https://doi.org/10.1016/j.orggeochem.2012.09.006>, 2013.

1047 Schouten, S., Villanueva, L., Hopmans, E. C., van der Meer, M. T. J. and Sinninghe Damsté, J. S.: Are
1048 Marine Group II Euryarchaeota significant contributors to tetraether lipids in the ocean?, *Proc. Natl. Acad.*
1049 *Sci. U. S. A.*, 111, 4285, <https://doi.org/10.1073/pnas.1416176111>, 2014.

1050 Schubotz, F., Wakeham, S. G., Lipp, J. S., Fredricks, H. F. and Hinrichs, K. U.: Detection of microbial
1051 biomass by intact polar membrane lipid analysis in the water column and surface sediments of the Black Sea,
1052 *Environ. Microbiol.*, 11, 2720–2734, <https://doi.org/10.1111/j.1462-2920.2009.01999.x>, 2009.

1053 Shah, S. R., Mollenhauer, G., Ohkouchi, N., Eglinton, T. I. and Pearson, A.: Origins of archaeal tetraether
1054 lipids in sediments: Insights from radiocarbon analysis, *Geochim. Cosmochim. Acta.*, 72, 4577–4594,
1055 <https://doi.org/10.1016/j.gca.2008.06.021>, 2008.

1056 Shepherd, A., Wingham, D. J., Mansley, J. A. D. and Corr, H. F. J.: Inland thinning of Pine Island Glacier,
1057 West Antarctica, *Science*, 291, 862–864, <https://doi.org/10.1126/science.291.5505.862>, 2001.

1058 Shevenell, A.E., Ingalls, A.E., Dormack, E.W. and Kelly, C.: Holocene Southern Ocean surface temperature
1059 variability west of the Antarctic Peninsula. *Nature*, 470, 250–254, <https://doi.org/10.1038/nature09751>, 2011.

1060 Signori, C.N., Pellizari, V.H., Enrich-Prast, A. and Sievert, S.M.: Spatiotemporal dynamics of marine
1061 bacterial and archaeal communities in surface waters off the northern Antarctic Peninsula, *Deep Sea Res.*
1062 *Part II Top. Stud. Oceanogr.*, 149, 150–160, <https://doi.org/10.1016/j.dsr2.2017.12.017>, 2018.

1063 Sinninghe Damsté, J.S., van Bentum, E.C., Reichart, G-J., Pross, J. and Schouten, S.: A CO₂ decrease-driven
1064 cooling and increased latitudinal temperature gradient during the mid-Cretaceous Oceanic Anoxic Event 2,
1065 *Earth Planet. Sci. Lett.* 293, 97–103, <https://doi.org/10.1016/j.epsl.2010.02.027>, 2010.

1066 Sinninghe Damsté, J. S., Rijpstra, W. I. C., Hopmans, E. C., Jung, M. Y., Kim, J. G., Rhee, S. K.,
1067 Stieglmeier, M. and Schleper, C.: Intact polar and core Glycerol Dibiphytanyl Glycerol Tetraether lipids of

1068 Group I.1a and I.1b Thaumarchaeota in soil, *Appl. Environ. Microbiol.*, 78, 6866–6874,
1069 <https://doi.org/10.1128/aem.01681-12>, 2012.

1070 Sinninghe Damsté, J. S., Rijpstra, W. I. C., Hopmans, E. C., den Uijl, M.J., Weijers, J.W.H., Schouten, S.
1071 The enigmatic structure of the crenarchaeol isomer, *Org. Geochem.*, 124, 22-28,
1072 <https://doi.org/10.1016/j.orggeochem.2018.06.005>, 2018.

1073 Smith, J.A., Andersen, T.J., Shortt, M., Truffer, M., Stanton, T.P., Bindschadler, R., Dutrieux, P., Jenkins,
1074 A., Hillenbrand, C.-D., Ehrmann, W., Corr, H.F.J., Farley, N., Crowhurst, S. and Vaughan, D.G.: Sub-ice-
1075 shelf sediments record history of 20th Century retreat of Pine Island Glacier. *Nature* 540, 77-80,
1076 <https://doi.org/10.1038/nature20136>. 2017.

1077 Sokolov, S. and Rintoul, S. R.: Circulation structure and distribution of the Antarctic Circumpolar Current
1078 fronts: 1. Mean circumpolar paths. *J. Geophys. Res.* 114, C11018, <https://doi.org/10.1029/2008JC005248>.
1079 2009.

1080 Sollai, M., Villanueva, L., Hopmans, E.C., Reichart, G-J., Sinninghe Damsté, J.S.: A combined lipidomic
1081 and 16S rRNA gene amplicon sequencing approach reveals archaeal sources of intact polar lipids in the
1082 stratified Black Sea water column, *Geobiology.*, 17, 91-109, <https://doi.org/10.1111/gbi.12316>, 2019a.

1083 Sollai, M., Villanueva, L., Hopmans, E.C., Keil, R.G., Sinninghe Damsté, J.S.: Archaeal sources of intact
1084 membrane lipid biomarkers in the oxygen deficient zone of the Eastern Tropical South Pacific, *Front.*
1085 *Microbiol.*, 10, <https://doi.org/10.3389/fmicb.2019.00765>, 2019b.

1086 Sollich, M., Yoshinaga, M. Y., Hausler, S., Price, R. E., Hinrichs, K. U. and Buhning, S. I.: Heat stress
1087 dictates microbial lipid composition along a thermal gradient in marine sediments, *Front. Microbiol.*, 8, 1-19
1088 <https://doi.org/10.3389/fmicb.2017.01550>, 2017.

1089 Spang, A., Hatzepichler, R., Brochier-Armanet, C., Rattei, T., Tischler, P., Spieck, E., Streit, W., Stahl, D.
1090 A., Wagner, M. and Schleper, C.: Distinct gene set in two different lineages of ammonia-oxidizing archaea
1091 supports the phylum Thaumarchaeota, *Trends Microbiol.*, 18, 331–340,
1092 <https://doi.org/10.1016/j.tim.2010.06.003>, 2010.

1093 St-Laurent, P., Yager, P. L., Sherrell, R. M., Stammerjohn, S. E. and Dinniman, M. S.: Pathways and supply
1094 of dissolved iron in the Amundsen Sea (Antarctica), *J. Geophys. Res. Oceans*, 122, 7135–7162,
1095 <https://doi.org/10.1002/2017JC013162>, 2017.

1096 Sturt, H. F., Summons, R. E., Smith, K., Elvert, M. and Hinrichs, K. U.: Intact polar membrane lipids in
1097 prokaryotes and sediments deciphered by high-performance liquid chromatography/electrospray ionization
1098 multistage mass spectrometry - new biomarkers for biogeochemistry and microbial ecology, *Rapid Commun.*
1099 *Mass Spectrom.*, 18, 617–628, <https://doi.org/10.1002/rcm.1378>, 2004.

1100 Thuroczy, C.-E., Alderkamp, A.-C., Laan, P., Gerringa, L. J. A., Mills, M. M., Van Dijken, G. L., De Baar,
1101 H. J. W. and Arrigo, K. R.: Key role of organic complexation of iron in sustaining phytoplankton blooms in
1102 the Pine Island and Amundsen Polynyas (Southern Ocean), *Deep-Sea Res. Part II- Top. Stud. Oceanogr.*, 71–
1103 76, 49–60, <https://doi.org/10.1016/j.dsr2.2012.03.009>, 2012.

1104 Tolar, B. B., Ross, M. J., Wallsgrove, N. J., Liu, Q., Aluwihare, L. I., Popp, B. N. and Hollibaugh, J. T.:
1105 Contribution of ammonia oxidation to chemoautotrophy in Antarctic coastal waters, *Isme J.*, 10, 2605–2619,
1106 <https://doi.org/10.1038/ismej.2016.61>, 2016.

1107 Venables, H. J.: JR272A Weddell and Scotia Sea hydrographic section, British Antarctic Survey, Cambridge,
1108 UK, https://www.bodc.ac.uk/resources/inventories/cruise_inventory/reports/jr272.pdf, 2012.

1109 Vernet, M., Geibert, W., Hoppema, M., Brown, P. J., Haas, C., Hellmer, H. H., Jokat, W., Jullion, L.,
1110 Mazloff, M., Bakker, D. C. E., Brearley, J. A., Croot, P., Hattermann, T., Hauck, J., Hillenbrand, C.-D.,
1111 Hoppe, C. J. M., Huhn, O., Koch, B. P., Lechtenfeld, O. J., Meredith, M. P., Naveira Garabato, A. C.,
1112 Nöthig, E.-M., Peeken, I., Rutgers van der Loeff, M. M., Schmidtko, S., Schröder, M., Strass, V. H., Torres-
1113 Valdés, S. and Verdy, A.: The Weddell Gyre, Southern Ocean: Present knowledge and future challenges,
1114 *Rev. Geophys.* 57, 623-708, <https://doi.org/10.1029/2018RG000604>, 2019.

1115 Wadham, J. L., De'ath, R., Monteiro, F. M., Tranter, M., Ridgwell, A., Raiswell, R. and Tulaczyk, S.: The
1116 potential role of the Antarctic Ice Sheet in global biogeochemical cycles, *Earth Environ. Sci. Trans. R. Soc.*
1117 *Edinb.*, 104, 55–67, <https://doi.org/10.1017/S1755691013000108>, 2013.

1118 Wadham, J. L., Hawkings, J. R., Tarasov, L., Gregoire, L. J., Spencer, R. G. M., Gutjahr, M., Ridgwell, A.
1119 and Kohfeld, K. E.: Ice sheets matter for the global carbon cycle., *Nat. Commun.*, 10, 1-17, [https://doi.org/](https://doi.org/10.1038/s41467-019-11394-4)
1120 10.1038/s41467-019-11394-4, 2019.

1121 Webber, B. G. M., Heywood, K. J., Stevens, D. P., Dutrieux, P., Abrahamsen, E. P., Jenkins, A., Jacobs, S.
1122 S., Ha, H. K., Lee, S. H., and Kim, T. W.: Mechanisms driving variability in the ocean forcing of Pine Island
1123 Glacier, *Nat. Commun.*, 8, [https://doi.org/ 14507](https://doi.org/14507), 10.1038/ncomms14507, 2017.

1124 [Weber, Y., Sinninghe Damsté, J.S., Hopmans, E.C., Lehmann, M.F. & Niemann, H.: Incomplete recovery of](http://10.1002/lom3.10198)
1125 [intact polar glycerol dialkyl glycerol tetraethers from lacustrine suspended biomass. *Limn. Oceanogr.*](http://10.1002/lom3.10198)
1126 [Methods. 15, 782-793. <http://10.1002/lom3.10198>. 2017.](http://10.1002/lom3.10198)

1127 Wilkins, D., Lauro, F. M., Williams, T. J., Demaere, M. Z., Brown, M. V., Hoffman, J. M., Andrews-
1128 Pfankoch, C., Mcquaid, J. B., Riddle, M. J., Rintoul, S. R. and Cavicchioli, R.: Biogeographic partitioning
1129 of Southern Ocean microorganisms revealed by metagenomics, *Environ. Microbiol.*, 15, 1318–1333,
1130 <https://doi.org/10.1111/1462-2920.12035>, 2013.

1131 Wingham, D. J., Wallis, D. W. and Shepherd, A.: Spatial and temporal evolution of Pine Island Glacier
1132 thinning, 1995-2006, *Geophys. Res. Lett.*, 36, 1-5, <https://doi.org/10.1029/2009gl039126>, 2009.

1133 Xie, S. T., Lipp, J. S., Wegener, G., Ferdelman, T. G. and Hinrichs, K-U.: Turnover of microbial lipid in the
1134 deep biosphere and growth of benthic archaeal populations, *PNAS*, 100, 6010-6014, [https://doi.org/](https://doi.org/10.1073/pnas.1218569110)
1135 10.1073/pnas.1218569110, 2013.

1136 Xie, S. T., Liu, X. L., Schubotz, F., Wakeham, S. G. and Hinrichs, K. U.: Distribution of glycerol ether lipids
1137 in the oxygen minimum zone of the Eastern Tropical North Pacific Ocean, *Org. Geochem.*, 71, 60–71,
1138 <https://doi.org/10.1016/j.orggeochem.2014.04.006>, 2014.

1139 Yager, P.L., Sherrell, R.M., Stammerjohn, S.E., Alderkamp, A.-C., Schofield, O., Abrahamsen, E.P., Arrigo,
1140 K.R., Bertilsson, S., Garay, D.L., Guerrero, R., Lowry, K.E., Moksnes, P.-O., Ndungu, K., Post, A.F.,
1141 Randall-Goodwin, E., Riemann, L., Severmann, S., Thatje, S., van Dijken, G.L. and Wilson, S.: ASPIRE:
1142 The Amundsen sea Polynya international research expedition. *Oceanography*, 25, 40-53, [https://doi.org/](https://doi.org/10.5670/oceanog.2012.73)
1143 10.5670/oceanog.2012.73. 2012.

- 1144 Zeng, Z., Liu, X-L., Farley, K. R., Wei, J. H., Metcalf, W. W., Summons, R. E. and Welander, P. V.: GDGT
1145 cyclization proteins identify the dominant archaeal sources of tetrarther lipids in the ocean. PNAS, 45,
1146 22505-22511, [https://doi.org/ 10.1073/pnas.1909306116](https://doi.org/10.1073/pnas.1909306116). 2019.
- 1147 Zhang, Y. G., Pagani, M. and Zhengrong, W.: Ring Index: A new strategy to evaluate the integrity of TEX86
1148 paleothermometry. *Paleoceanography*, 31, 220-232, [https://doi.org/ 10.1002/2015PA002848](https://doi.org/10.1002/2015PA002848). 2016.
- 1149 Zhu, C., Wakeham, S. G., Elling, F. J., Basse, A., Mollenhauer, G., Versteegh, G. J. M., Konneke, M. and
1150 Hinrichs, K. U.: Stratification of archaeal membrane lipids in the ocean and implications for adaptation and
1151 chemotaxonomy of planktonic archaea, *Environ. Microbiol.*, 18, 4324–4336, [https://doi.org/10.1111/1462-](https://doi.org/10.1111/1462-2920.13289)
1152 2920.13289, 2016.
- 1153 Zwally, H. J., Giovinetto, M. B., Li, J., Cornejo, H. G., Beckley, M. A., Brenner, A. C., Saba, J. L. and Yi,
1154 D. H.: Mass changes of the Greenland and Antarctic ice sheets and shelves and contributions to sea-level
1155 rise: 1992-2002, *J. Glaciol.*, 51, 509–527, <https://doi.org/10.3189/172756505781829007>, 2005.

1156 Table 1: Scotia Sea SPM samples studied and their physical properties including sample depth (m) and
 1157 sample layer where “M” denotes mixed layer and “T” denotes thermocline layer, GDGT-0/cren, and Ring
 1158 Index. ~~(figures to 2 decimal places (d.p.)).~~

Latitude (°N)	Longitude (°E)	Station	Sample Depth (m)	Layer	Temperature (°C)	Salinity (PSU)	Fluorescence (ml/m ³)	<u>GDGT- 0/Cren</u>	<u>Ring Index</u>
-53.013	-58.04	CTD 1	15	M	7.31	33.99	0.41	<u>2.6</u>	<u>0.9</u>
-53.013	-58.04	CTD 1	100	T	6.12	34.03	0.13	<u>6.7</u>	<u>0.4</u>
-53.586	-42.835	CTD 23	20	M	4.07	33.72	0.32		
-53.586	-42.835	CTD 23	100	T	2.23	33.81	0.08	<u>1.8</u>	<u>0.7</u>
-52.88	-41.787	CTD 24	15	M	3.55	33.72	1.09		
-52.88	-41.787	CTD 24	80	T	1.67	33.88	0.09	<u>1.6</u>	<u>0.9</u>
-53.743	-38.155	CTD 25	10	M	3.17	33.62	0.66		
-53.743	-38.155	CTD 25	80	T	1.95	33.91	0.05	<u>2.4</u>	<u>0.8</u>
-57.119	-31.815	CTD 22	30	M	1.34	33.82	0.24		
-56.167	-34.816	CTD 22	110	T	0.84	34.12	0.09	<u>1.9</u>	<u>0.5</u>
-57.459	-31.327	CTD 21	30	M	1.48	33.85	0.27		
-57.459	-31.327	CTD 21	110	T	1.34	34.3	0.03	<u>5.3</u>	<u>0.2</u>
-57.803	-30.83	CTD 20	30	M	1.60	33.92	0.28	<u>2.2</u>	<u>1.0</u>
-57.803	-30.83	CTD 20	110	T	1.01	34.15	0.06	<u>6.8</u>	<u>0.2</u>
-58.213	-30.822	CTD 19	20	M	1.29	33.9	0.27		
-58.213	-30.822	CTD 19	80	T	1.16	34.19	0.09	<u>8.0</u>	<u>0.3</u>
-58.624	-30.821	CTD 18	20	M	0.65	33.69	0.17		
-58.624	-30.821	CTD 18	90	T	-0.83	33.99	0.17	<u>4.1</u>	<u>0.6</u>
-59.436	-30.861	CTD 16	20	M	-0.64	33.67	0.17		
-59.436	-30.861	CTD 16	70	T	-1.32	34.12	0.08	<u>16.8</u>	<u>1.0</u>
-60.319	-30.961	CTD 13	30	M	-0.89	33.74	0.11		
-60.319	-30.961	CTD 13	65	T	-1.16	34.01	0.11	<u>4.6</u>	<u>0.6</u>
-61.171	-31.045	CTD 10	30	M	-1.08	33.82	0.15		
-61.171	-31.045	CTD 10	80	T	-1.08	34.23	0.11	<u>177.6</u>	<u>0.02</u>
-62.084	-31.174	CTD 7	40	M	-1.11	33.87	0.4		
-62.084	-31.174	CTD 7	75	T	-1.54	34.33	0.16	<u>21.7</u>	<u>0.1</u>
-62.784	-30.706	CTD 5	20	M	-1.13	33.87	0.28		
-62.784	-30.706	CTD 5	70	T	-1.49	34.34	0.14	<u>4.3</u>	<u>0.7</u>
-63.346	-29.569	CTD 3	20	M	-1.18	33.8	0.22		
-63.346	-29.569	CTD 3	60	T	-1.58	34.31	0.21	<u>9.9</u>	<u>0.3</u>

1159

1160 Table 2: Amundsen Sea SPM samples studied and their physical properties (~~figures to 2 d.p.~~, GDGT-0/cren.
 1161 and Ring Index.

Latitude (° N)	Longitude (°E)	Station	Sample Depth (m)	Temperature (°C)	Salinity (PSU)	Fluorescence (ml/m ³)	<u>GDGT- 0/Cren</u>	<u>Ring Index</u>
-74.958	-101.829	PS104/003-1	10	-0.72	33.96	0.48	<u>7.3</u>	<u>0.5</u>
-74.958	-101.829	PS104/003-1	120	-1.19	34.13	0.01	<u>4.8</u>	<u>0.5</u>
-74.958	-101.829	PS104/003-1	180	-1.23	34.17	0.01	<u>27.0</u>	<u>0.03</u>
-74.958	-101.829	PS104/003-1	998	1.01	34.67	-0.02	<u>4.8</u>	<u>0.7</u>
-74.866	-100.76	PS104/007-1	20	-0.12	33.52	3.78	<u>8.2</u>	<u>0.4</u>
-74.866	-100.76	PS104/007-1	120	-0.91	34.08	0.01	<u>4.9</u>	<u>0.5</u>
-74.866	-100.76	PS104/007-1	240	-1.33	34.14	-0.01	<u>5.0</u>	<u>0.4</u>
-74.866	-100.76	PS104/007-1	685	0.87	34.63	-0.02	<u>4.2</u>	<u>0.6</u>
-74.359	-101.747	PS104/017-1	10	-0.17	33.42	7.89		
-74.359	-101.747	PS104/017-1	150	-1.61	34.16	0.01	<u>5.8</u>	<u>0.3</u>
-74.359	-101.747	PS104/017-1	1375	1.06	34.71	-0.02	<u>2.8</u>	<u>0.9</u>
-72.768	-107.093	PS104/022-1	10	-0.59	33.13	1.09		
-72.768	-107.093	PS104/022-1	30	-0.47	33.27	1.71		
-72.768	-107.093	PS104/022-1	120	-1.54	34.1	0.07	<u>3.8</u>	<u>0.6</u>
-72.768	-107.093	PS104/022-1	697	0.98	34.71	-0.02	<u>4.2</u>	<u>0.6</u>
-73.297	-112.328	PS104/043-2	10	-1.34	32.82	1.51		
-73.297	-112.328	PS104/043-2	120	-1.62	34.18	0.01	<u>3.3</u>	<u>0.5</u>
-73.297	-112.328	PS104/043-2	454	0.15	34.51	-0.02	<u>5.4</u>	<u>0.5</u>

1162

1163 Table 43: Relative abundances (%) and heat map of IPLs identified in Amundsen Sea. Relative abundances

1164 >30% indicated in red, low relative abundances <10% indicated in green. nd = not detected.

Station	Depth (cm)	GDGT-0			GDGT-1	GDGT-2	Crenarchaeol			OH-GDGT-0			diOH- GDGT-0
		MH	DH	HPH	DH	DH	MH	DH	HPH	MH	DH	HPH	MH
PS104/003-1	10	1.2	nd	81.8	nd	nd	0.2	nd	11.1	0.4	5.1	nd	0.2
PS104/003-1	120	0.6	2.2	56.2	1.5	nd	0.3	0.1	11.7	4.9	16.5	0.5	5.5
PS104/003-1	180	1.4	nd	18.0	nd	nd	0.7	nd	nd	24.1	25.7	nd	30.1
PS104/003-1	998	3.4	11.3	28.1	14.7	8.2	1.7	3.0	4.3	5.2	18.8	nd	1.3
PS104/007-1	20	89.1	nd	nd	nd	nd	10.9	nd	nd	nd	nd	nd	nd
PS104/007-1	120	1.4	4.6	38.8	5.1	1.9	1.0	0.4	7.7	6.9	25.7	nd	6.5
PS104/007-1	240	2.3	5.7	40.0	3.3	nd	1.3	nd	8.3	11.8	11.9	nd	15.4
PS104/007-1	685	1.3	8.9	37.8	9.1	4.1	1.3	1.8	8.3	3.6	22.7	nd	1.1
PS104/017-1	10	nd	nd	nd	nd	nd	nd	nd	nd	nd	nd	nd	nd
PS104/017-1	150	1.7	nd	43.9	nd	nd	1.0	nd	6.8	14.1	13.0	nd	19.5
PS104/017-1	1375	0.9	6.5	38.2	11.1	7.3	1.1	3.0	11.9	2.4	17.3	nd	0.3
PS104/022-1	10	nd	nd	nd	nd	nd	nd	nd	nd	nd	nd	nd	nd
PS104/022-1	30	nd	nd	nd	nd	nd	nd	nd	nd	nd	nd	nd	nd
PS104/022-1	120	2.8	nd	51.6	nd	nd	1.7	nd	12.4	11.1	9.3	1.2	9.9
PS104/022-1	697	4.3	6.0	31.5	11.2	5.3	2.0	2.3	5.6	5.5	25.0	nd	1.2
PS104/043-2	10	nd	nd	nd	nd	nd	nd	nd	nd	nd	nd	nd	nd
PS104/043-2	120	1.6	nd	38.3	nd	nd	0.5	nd	11.5	4.6	37.9	0.9	4.7
PS104/043-2	454	0.7	0.2	72.3	nd	nd	0.2	nd	13.2	1.7	8.6	0.7	2.4

1165

1166 Table 34: Relative abundances (%) and heat map of IPLs identified in Scotia Sea. Relative abundances >30%
 1167 indicated in red, low relative abundances <10% indicated in green. nd = not detected.

CTD	Depth (m)	GDGT-0			GDGT-1	Crenarchaeol			OH-GDGT-0			diOH-GDGT-0
		MH	DH	HPH	DH	MH	DH	HPH	MH	DH	HPH	MH
1	15	6.8	nd	49.6	nd	3.4	nd	18.6	nd	21.6	nd	nd
1	100	4.6	nd	54.9	nd	3.3	nd	5.6	2.6	28.2	nd	0.8
23	20	nd	nd	nd	nd	nd	nd	nd	nd	nd	nd	nd
23	100	31.0	nd	nd	nd	16.8	nd	nd	19.6	17.7	nd	14.9
24	15	nd	nd	nd	nd	nd	nd	nd	nd	nd	nd	nd
24	80	36.2	nd	1.6	nd	23.3	nd	nd	16.5	15.7	nd	6.7
25	10	nd	nd	nd	nd	nd	nd	nd	nd	nd	nd	nd
25	80	10.1	1.0	35.3	nd	6.1	nd	13.4	8.7	14.8	1.8	8.8
22	30	nd	nd	nd	nd	nd	nd	nd	nd	nd	nd	nd
22	110	13.5	nd	8.8	nd	11.9	nd	nd	21.7	23.7	nd	20.4
21	30	52.6	nd	nd	nd	nd	nd	nd	47.4	nd	nd	nd
21	110	9.3	4.0	10.2	3.5	4.5	nd	nd	11.8	35.3	nd	21.4
20	30	53.0	nd	nd	nd	24.5	nd	nd	22.5	nd	nd	nd
20	110	9.0	nd	31.8	nd	6.0	nd	nd	12.4	28.2	nd	12.6
19	20	nd	nd	nd	nd	nd	nd	nd	nd	nd	nd	nd
19	80	3.1	nd	55.7	nd	2.6	nd	4.8	6.4	19.2	nd	8.2
18	20	nd	nd	nd	nd	nd	nd	nd	nd	nd	nd	nd
18	90	4.2	nd	57.8	nd	1.9	nd	13.4	4.7	9.2	2.6	6.2
16	20	nd	nd	100.0	nd	nd	nd	nd	nd	nd	nd	nd
16	70	7.8	nd	45.9	nd	3.2	nd	nd	20.6	8.9	nd	13.6
13	30	nd	nd	nd	nd	nd	nd	nd	nd	nd	nd	nd
13	65	15.3	nd	54.2	nd	4.1	nd	11.1	10.5	nd	nd	4.8
10	30	nd	nd	nd	nd	nd	nd	nd	nd	nd	nd	nd
10	80	4.2	nd	82.6	nd	0.5	nd	nd	7.0	nd	nd	5.7
7	40	nd	nd	nd	nd	nd	nd	nd	nd	nd	nd	nd
7	75	7.2	nd	47.7	nd	2.5	nd	nd	29.8	nd	nd	12.7
5	20	nd	nd	nd	nd	nd	nd	nd	nd	nd	nd	nd
5	70	0.7	nd	71.1	nd	0.4	nd	16.3	2.3	4.8	2.5	1.9
3	20	nd	nd	nd	nd	nd	nd	nd	nd	nd	nd	nd
3	60	45.2	nd	22.7	nd	6.9	nd	nd	25.2	nd	nd	nd

1168

1169 ~~Table 4: Relative abundances (%) and heat map of IPLs identified in Amundsen Sea. Relative abundances~~
 1170 ~~≥30% indicated in red, low relative abundances <10% indicated in green. nd = not detected.~~

Station	Depth (cm)	GDGT-0			GDGT-1	GDGT-2	Crenarchaeol			OH-GDGT-0			diOH- GDGT-0
		MH	DH	HPH	DH	DH	MH	DH	HPH	MH	DH	HPH	MH
PS104/003-1	10	1.2	nd	81.8	nd	nd	0.2	nd	11.1	0.4	5.1	nd	0.2
PS104/003-1	120	0.6	2.2	56.2	1.5	nd	0.3	0.1	11.7	4.9	16.5	0.5	5.5
PS104/003-1	180	1.1	nd	18.0	nd	nd	0.7	nd	nd	24.1	25.7	nd	30.1
PS104/003-1	998	3.1	11.3	28.1	14.7	8.2	1.7	3.0	4.3	5.2	18.8	nd	1.3
PS104/007-1	20	89.1	nd	nd	nd	nd	10.9	nd	nd	nd	nd	nd	nd
PS104/007-1	120	1.1	4.6	38.8	5.1	1.9	1.0	0.1	7.7	6.9	25.7	nd	6.5
PS104/007-1	240	2.3	5.7	40.0	3.3	nd	1.3	nd	8.3	11.8	11.9	nd	15.4
PS104/007-1	685	1.3	8.9	37.8	9.1	4.1	1.3	1.8	8.3	3.6	22.7	nd	1.1
PS104/017-1	10	nd	nd	nd	nd	nd	nd	nd	nd	nd	nd	nd	nd
PS104/017-1	150	1.7	nd	43.9	nd	nd	1.0	nd	6.8	14.1	13.0	nd	19.5
PS104/017-1	1375	0.9	6.5	38.2	11.1	7.3	1.1	3.0	11.9	2.1	17.3	nd	0.3
PS104/022-1	10	nd	nd	nd	nd	nd	nd	nd	nd	nd	nd	nd	nd
PS104/022-1	30	nd	nd	nd	nd	nd	nd	nd	nd	nd	nd	nd	nd
PS104/022-1	120	2.8	nd	51.6	nd	nd	1.7	nd	12.4	11.1	9.3	1.2	9.9
PS104/022-1	697	4.3	6.0	31.5	11.2	5.3	2.0	2.3	5.6	5.5	25.0	nd	1.2
PS104/043-2	10	nd	nd	nd	nd	nd	nd	nd	nd	nd	nd	nd	nd
PS104/043-2	120	1.6	nd	38.3	nd	nd	0.5	nd	11.5	4.6	37.9	0.9	4.7
PS104/043-2	454	0.7	0.2	72.3	nd	nd	0.2	nd	13.2	1.7	8.6	0.7	2.1

1171

1173 Table 5: Ratios of monohexose/dihexose (MH/DH), monohexose/hexosephosphohexose (MH/HPH), GDGT-
 1174 0/crenarchaeol (GDGT-0/Cren), and Ring Index in the Scotia Sea.

Sea	Station	Depth (cm)	MH/DH	MH/HPH	GDGT-0/Cren	Ring Index
Scotia	CTD-1	15	0.5	0.1	2.6	0.9
Scotia	CTD-1	100	0.4	0.2	6.7	0.4
Scotia	CTD-23	20				
Scotia	CTD-23	100	4.7		1.8	0.7
Scotia	CTD-24	15				
Scotia	CTD-24	80	5.3	52.4	1.6	0.9
Scotia	CTD-25	10				
Scotia	CTD-25	80	2.1	0.7	2.4	0.8
Scotia	CTD-22	30				
Scotia	CTD-22	110	2.8	7.7	1.9	0.5
Scotia	CTD-21	30				
Scotia	CTD-21	110	1.1	4.6	5.3	0.2
Scotia	CTD-20	30			2.2	1.0
Scotia	CTD-20	110	1.4	1.3	6.8	0.2
Scotia	CTD-19	20				
Scotia	CTD-19	80	1.1	0.3	8.0	0.3
Scotia	CTD-18	20				
Scotia	CTD-18	90	1.8	0.2	4.1	0.6
Scotia	CTD-16	20				
Scotia	CTD-16	70	5.1	1.0	16.8	1.0
Scotia	CTD-13	30				
Scotia	CTD-13	65		0.5	4.6	0.6
Scotia	CTD-10	30				
Scotia	CTD-10	80		0.2	177.6	0.02
Scotia	CTD-7	40				
Scotia	CTD-7	75		1.1	21.7	0.1
Scotia	CTD-5	20				
Scotia	CTD-5	70	1.1	0.1	4.3	0.7
Scotia	CTD-3	20				
Scotia	CTD-3	60		3.4	9.9	0.3

1175

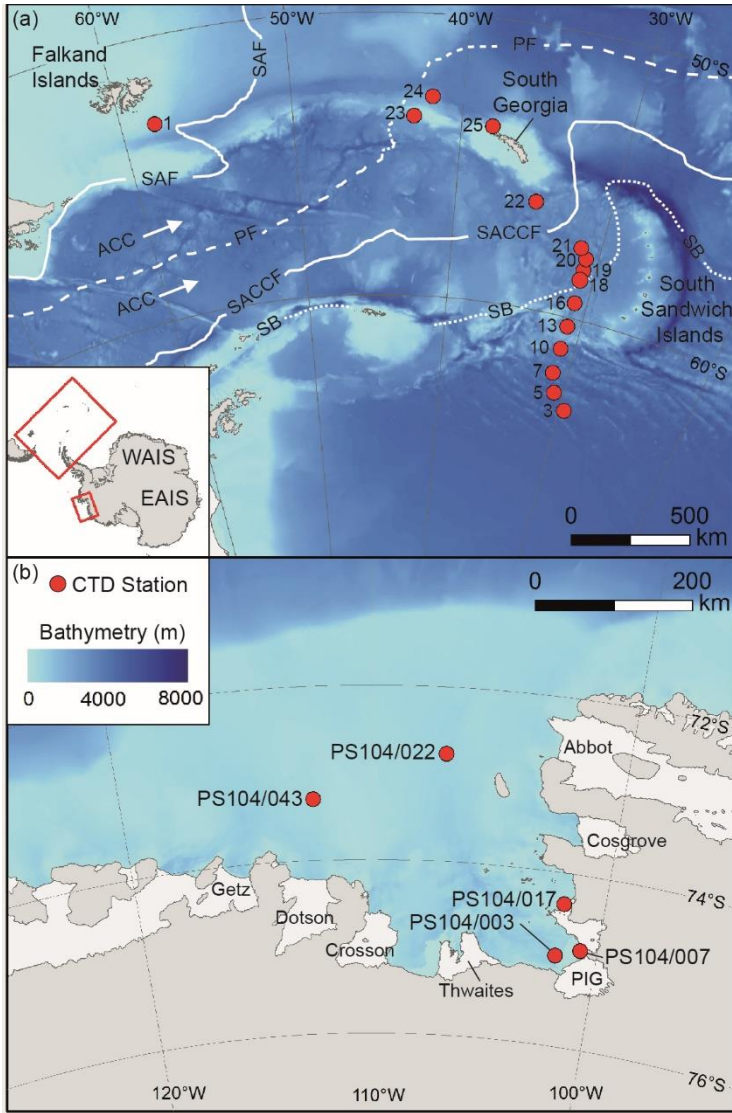
1176 Table 6: Ratios of monohexose/dihexose (MH/DH), monohexose/hexosephosphohexose (MH/HPH),
 1177 GDGT-0/crenarchaeol (GDGT-0/Cren), and Ring Index in the Amundsen Sea.

Sea	Station	Depth (cm)	MH/DH	MH/HPH	GDGT-0/Cren	Ring Index
Amundsen	PS104/003-1	10	0.4	0.0	7.3	0.5
Amundsen	PS104/003-1	120	0.6	0.2	4.8	0.5
Amundsen	PS104/003-1	180	2.2	3.1	27.0	0.03
Amundsen	PS104/003-1	998	0.2	0.4	4.8	0.7
Amundsen	PS104/007-1	20			8.2	0.4
Amundsen	PS104/007-1	120	0.4	0.3	4.9	0.5
Amundsen	PS104/007-1	240	1.5	0.6	5.0	0.4
Amundsen	PS104/007-1	685	0.2	0.2	4.2	0.6
Amundsen	PS104/017-1	10				
Amundsen	PS104/017-1	150	2.8	0.7	5.8	0.3
Amundsen	PS104/017-1	1375	0.1	0.1	2.8	0.9
Amundsen	PS104/022-1	10				
Amundsen	PS104/022-1	30				
Amundsen	PS104/022-1	120	2.8	0.4	3.8	0.6
Amundsen	PS104/022-1	697	0.3	0.4	4.2	0.6
Amundsen	PS104/043-2	10				
Amundsen	PS104/043-2	120	0.3	0.2	3.3	0.5
Amundsen	PS104/043-2	454	0.6	0.1	5.4	0.5

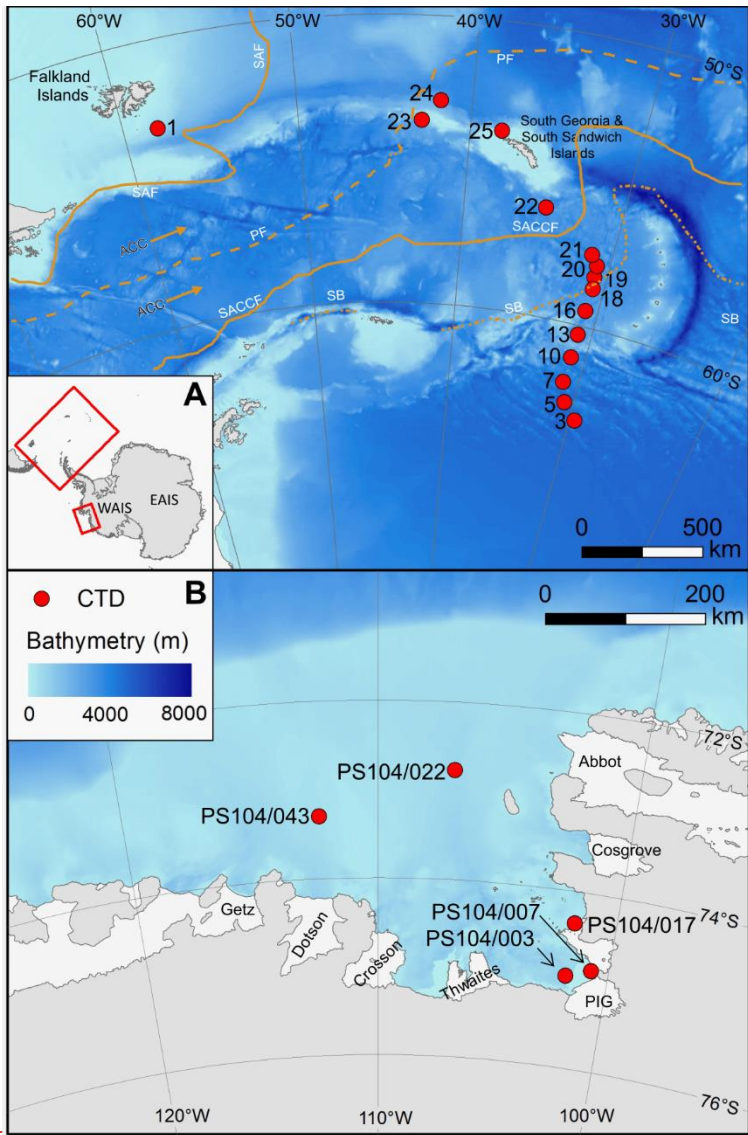
1178

1179

1180 Figure 1. Map showing studied CTD sampling stations (red dots) in the Scotia sea (A) and Amundsen sea
 1181 (B). The main oceanic fronts are also shown in panel A; subantarctic (SAF), polar (PF), southern ACC
 1182 (SACCF) and the southern boundary of the ACC (SB) (Sokolov and Rintoul, 2009). The names of the ice
 1183 shelves are shown in panel B.

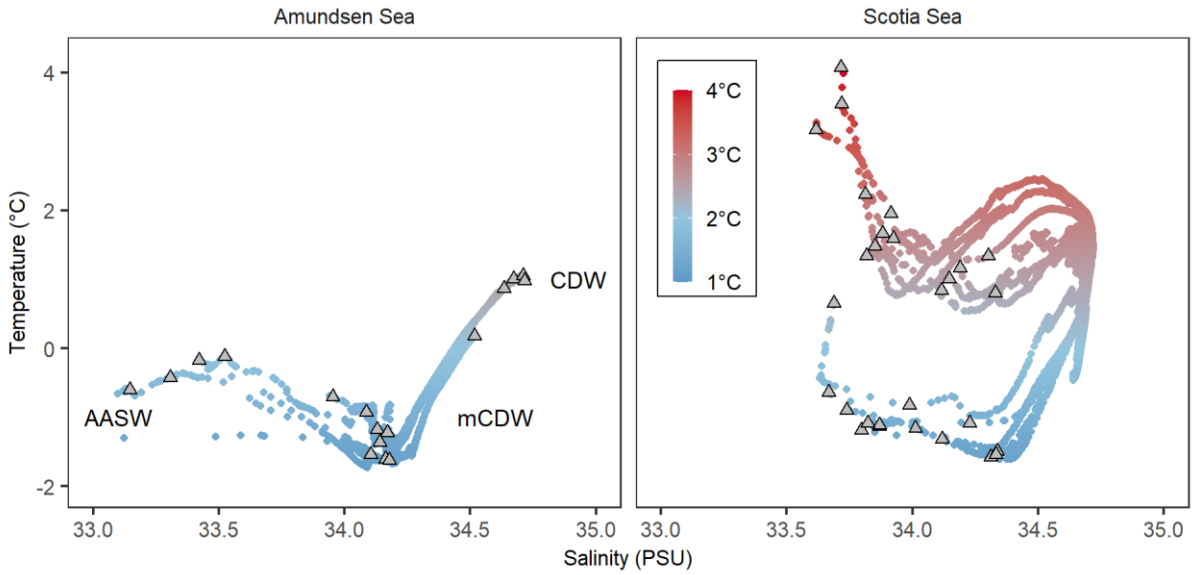


1184

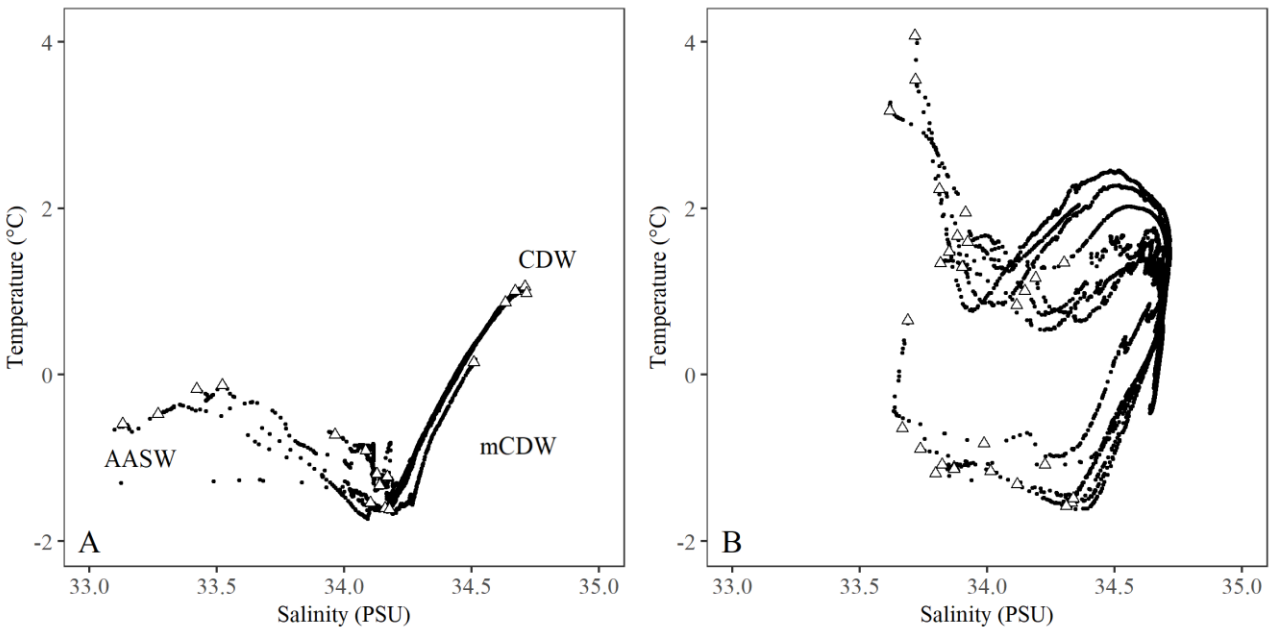


1185

1186 Figure 2. The TTemperature and Ssalinity profiles (T-S plot) for the Amundsen Sea (A) showing Antarctic
 1187 Surface Water (AASW) and Circumpolar Deep Water (CDW), and Scotia Sea (B). Coloured circles indicate
 1188 the water column temperature of the water massesBlack dots indicate the CTD data and with the open-grey
 1189 triangles indicate the seawater-water column sampling depths.

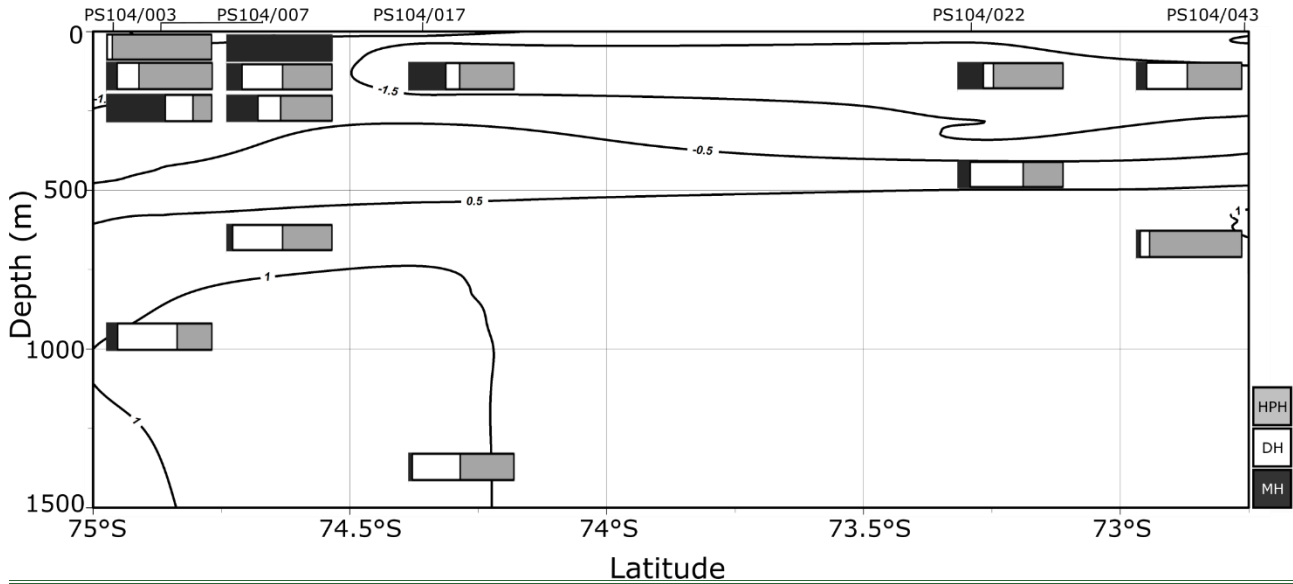


1190



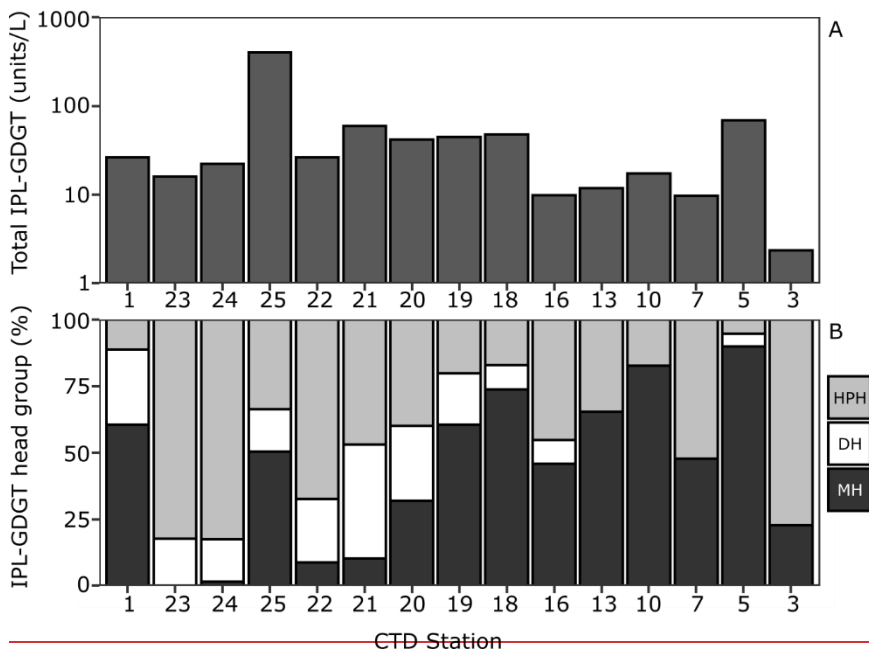
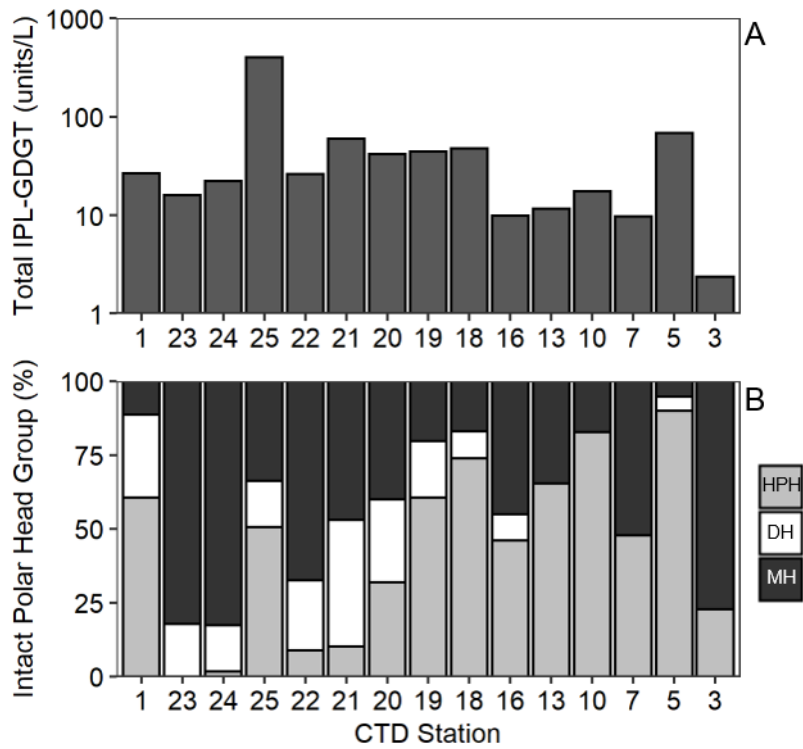
1191

1192 Figure 34. Relative abundance (%) of intact GDGTs at approximate sample depths in the Amundsen Sea.
1193 Bars reflect intact-GDGT head group with black representing MH head groups, white representing DH, and
1194 grey representing HPH. Contour lines show approximate ocean temperature ranges using CTD data taken at
1195 each sample station with Ocean Data View DIVA gridding.



1196

1197 Figure 34. Total IPL-GDGT concentration (Log_{10} , units/L) (A) and relative abundance (%) of IPL head
 1198 groups, monohexose (MH, black), dihexose (DH, white), hexose-phosphohexose (HPH, grey) (B) in Scotia
 1199 Sea thermocline samples (mixed layer samples excluded from plots).



1200

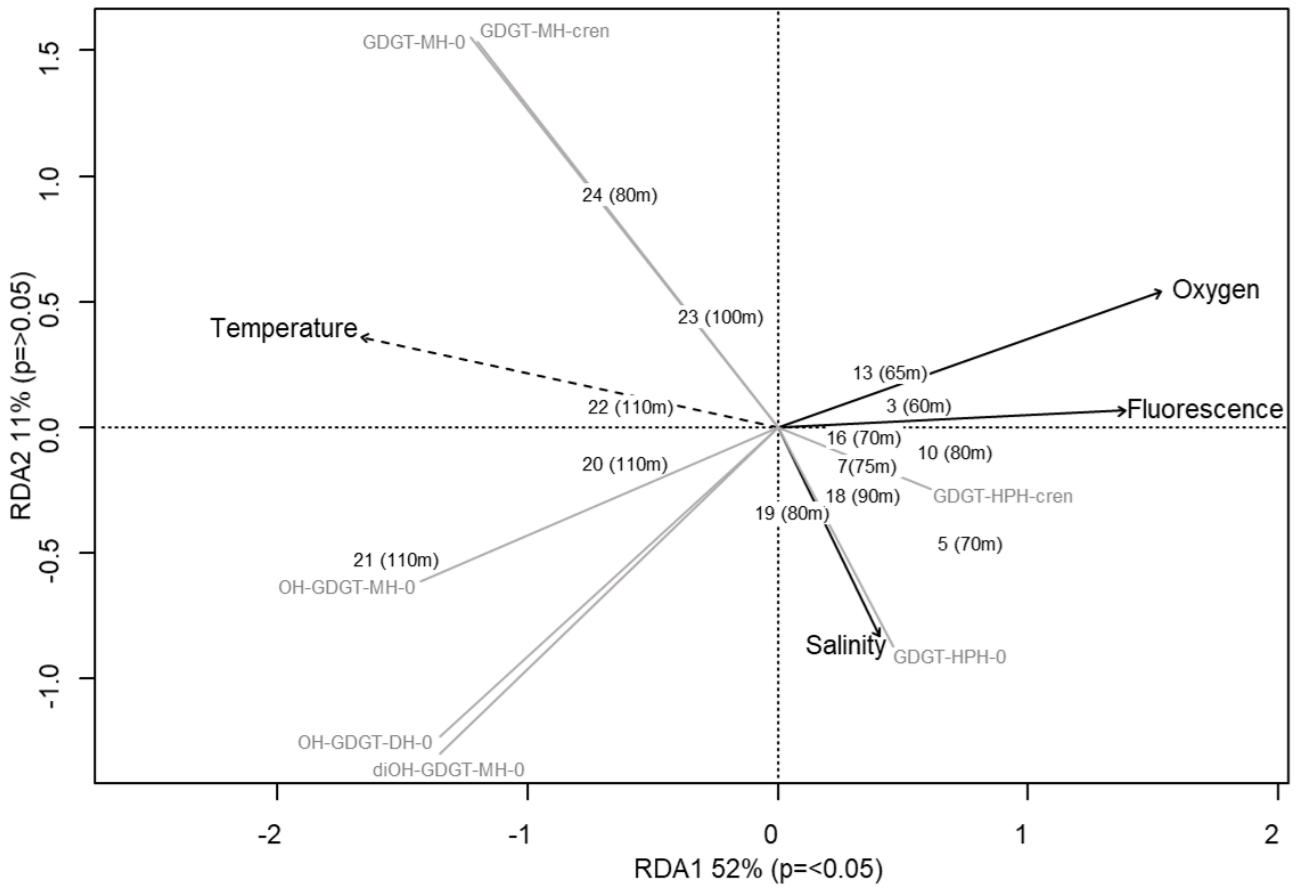
1201

1202 Figure 4. Relative abundance (%) of intact GDCTs at approximate sample depths in the Amundsen Sea. Bars
1203 reflect intact GDCT head group with black representing MH head groups, white representing DH, and grey
1204 representing HPH. Contour lines show approximate ocean temperature ranges using CTD data taken at each
1205 sample station with Ocean Data View DIVA gridding.



1206

1207 Figure 5. Redundancy analysis triplot for Scotia Sea sample set showing samples with depths, biomarker
 1208 response variables (grey lines), and explanatory variables (black with dashed lines indicating statistical
 1209 significance).



1210

1211 Supplement A. Absolute masses of IPLS detected in this study including for GDGTs, OH-GDGTs, and
1212 diOH-GDGTs with either MH, DH, or HPH head groups, and for each adduct (H⁺, NH₄⁺, and Na⁺).

1213 Supplement B: S12. Intact GDGT structures showing GDGT cores where, GDGT: R & R' = H; OH-GDGT:
1214 R=OH, R'=H; diOH-GDGT: R & R' = OH. Monohexose (MH), dihexose (DH), and hexose-phosphohexose
1215 (HPH) polar head groups structures shown.

1216 S21. CTD matrix showing temperature (°C), salinity (PSU), chlorophyll fluorescence (mg/m³), dissolved
1217 Oxygen (μmol/kgm/L) for CTD stations PS104/003 (A), PS104/007 (B), PS104/017 (C), PS104/022 (D),
1218 PS104/043 (E), with seawater sample depths indicated by a triangle.

1219 ~~S2. Intact GDGT structures showing GDGT cores where, GDGT: R & R' = H; OH-GDGT: R=OH, R'=H;~~
1220 ~~diOH-GDGT: R & R' = OH. Monohexose (MH), dihexose (DH), and hexose-phosphohexose (HPH) polar~~
1221 ~~head groups structures shown.~~

1222 Supplement C. Redundancy analysis output for Scotia Sea sample set including ANOVA.